# Investigating Drivers of Chemoresistance in Small Cell Lung Cancer

Eli Grunblatt

A dissertation

submitted in partial fulfillment of the

requirements for the degree of

Doctor of Philosophy

University of Washington

2020

Reading Committee:

David P. MacPherson, Chair

Elizabeth A. Nance

Mary Claire King

Program Authorized to Offer Degree:

Molecular and Cellular Biology

University of Washington

## Abstract

Investigating Drivers of Chemoresistance in Small Cell Lung Cancer

Eli Grunblatt

Chair of the Supervisory Committee:

David P. MacPherson, Associate Member

Division of Human Biology, Fred Hutchinson Cancer Research Center

Small cell lung cancer (SCLC) is an aggressive neuroendocrine cancer characterized by initial chemosensitivity followed by rapid emergence of chemoresistant disease. To study the role of *MYC* family members in SCLC chemoresistance we utilized genetically engineered mouse models of SCLC and found that *MYCN* and *MYCL* overexpression abrogated response to cisplatin-etoposide chemotherapy. We extended these data to genetically perturb chemosensitive patient derived xenograft (PDX) models of SCLC. In chemosensitive PDX models, overexpression of either *MYCN* or *MYCL* also conferred a switch to chemoresistance. To investigate therapeutic strategies for *MYCN*-overexpressing SCLC, we utilized a genome-scale CRISPR-Cas9 sgRNA screen and identified the deubiquitinase USP7 as a *MYCN*-associated synthetic vulnerability. Pharmacological inhibition of USP7 re-sensitized chemoresistant *MYCN*-overexpressing PDX models to chemotherapy in vivo. Our findings show that MYC family member overexpression drives SCLC chemoresistance and provide a therapeutic strategy to restore chemosensitivity. To further investigate drivers of SCLC chemoresistance

beyond MYC family members we designed and built a small, focused sgRNA library targeting key genes of interest in SCLC. Using chemosensitive PDX models, we performed in vivo CRISPR-Cas9 sgRNA screens both on a genome-wide scale and on a smaller scale using our focused library. These screens identified several candidate genes and pathways, most notably the SAGA complex, for validation as potential drivers of chemoresistance in SCLC.

A version of portions of chapters 1, 2, 4, and 5 is currently in preparation as a journal article entitled:

*MYCN* drives chemoresistance in small cell lung cancer while USP7 inhibition can restore sensitivity

Eli Grunblatt, Nan Wu, Huajia Zhang, Xiaoli Liu, Justin P. Norton, Yamini Ohol, Paul Leger, Emily C. Eastwood, Rhiana Thomas, Ali H. Ibrahim, Deshui Jia, Ryan Basom, Keith Eaton, Renato Martins, A. McGarry Houghton, and David P. MacPherson

## Acknowledgements

I would like to thank my amazing doctoral advisor, David MacPherson, for guiding and supporting me over the course of the last 5 years. His dedication, diligence and enthusiasm have pushed me to develop my critical thinking skills and grow as a scientist. Thanks to the members past and present of the MacPherson Lab: Arnaud Augert, Justin Norton, Emily Eastwood, Joe Hiatt, Ali Ibrahim, Nan Wu, Deshui Jia, Jessica Huszar, Andrew Snyder, and Holly Sandborg for being wonderful, supportive colleagues who made the lab an enjoyable and stimulating workplace. Thanks to Patrick Paddison for being an incredible co-mentor and thanks to the members of the Paddison Lab: Dan Kuppers, Pia Hollerbauer, Lucas Carter, Heather Feldman, Tobi Bonifert, Jake Herman, Sonali Arora, and Anca Mihalis for insightful suggestions and great friendship. Thanks to the staff and leaders of the Medical Scientist Training Program (MSTP) for being willing to take a chance on me and for being an amazing source of support for the last 6 years. Thanks to the members of my thesis committee: Elizabeth Nance, Mary Claire King, and McGarry Houghton for providing me with sage advice, constructive criticisms, and resolute support. Special thanks to my first research mentor, Sumanta Goswami, for sparking my interest in biomedical research and starting me on my path to becoming a physician-scientist. Finally, I would like to thank all my friends and family for their heartfelt encouragement and companionship throughout this journey.

## Table of Contents

## List of Figures

## List of Tables

# CHAPTER 1- Introduction

## 1.1 Clinical Overview of Small Cell Lung Cancer

Small cell lung cancer (SCLC) is a highly aggressive carcinoma that accounts for approximately 35,000 new cases annually in the United States alone. SCLC is heavily associated with cigarette smoking, nearly all patients have a history of significant tobacco use (Byers 2015, Bunn 2016, Rudin 2019, Poirier 2020). Clinically, SCLC cases are classified as either limited stage or extensive stage disease depending on the size of the primary tumor at presentation and the presence or absence of distal metastases. While some patients who present with limited stage disease are candidates for radiation therapy, the standard of care for most SCLC patients is treatment with chemotherapy consisting of a platinum compound (such as carboplatin or cisplatin) in conjunction with a topoisomerase inhibitor such as etoposide (Rossi 2012). Initially, the majority of patients respond well to platinum- based chemotherapy, with many exhibiting near complete tumor regression upon treatment. However, these responses are typically transient, and tumors frequently return months later. Furthermore, these relapsed tumors are generally resistant to chemotherapy, leading to poor prognoses for patients. The overall 5 year survival rate for SCLC is currently less than 5%, making it one of the deadliest forms of cancer in the United States (Rossi 2012, Byers 2015). Despite decades of research, there have been minimal advances in the development of targeted therapies for SCLC. Recently, the combination of immune checkpoint inhibitors with a chemotherapy doublet received FDA approval, marking the first major change to SCLC treatment guidelines in almost 30 years (Horn 2018, Paz-Ares 2019).

Nonetheless, many SCLC patients do not respond to immunotherapy and the overall prognosis of SCLC remains dismal, in large part due to the aforementioned development of recalcitrant, chemoresistant disease (Horn 2018, Pacheco 2019, Paz-Ares 2019). As such, understanding and targeting the drivers of SCLC chemoresistance is of paramount importance.

### 1.2 Molecular Features of Small Cell Lung Cancer

SCLC is a neuroendocrine carcinoma that was initially thought to arise solely from pulmonary neuroendocrine cells (PNEC), a rare population of cells found in the central airways of the lung (Park 2011, Sutherland 2011). In recent years, it has been shown that SCLC can also arise from other cell types present in the lung epithelia exhibiting molecular features distinct from PNECs (Yang 2018). Furthermore, there are rare cases where SCLC can arise from transformed non-small cell lung cancer (NSCLC), potentially as a response to EGFR-specific targeted therapies (Oser 2015). Recent studies have shown that SCLC can be broadly classified into different subtypes based on differential expression of key transcription factors. The 2 most commonly observed subtypes are the neuroendocrine subtype, also referred to as classic SCLC, defined by high expression levels of the achaete-scute homolog 1 (*ASCL1*) transcription factor, and the neural subtype, also referred to as variant SCLC, defined by high expression levels of the neurogenic differentiation factor 1 (*NEUROD1*) transcription factor (Borromeo 2016, Rudin 2019). Other recently discovered, less commonly observed subtypes of SCLC include variants characterized by low levels of both *ASCL1* and *NEUROD1* expression and high expression levels of either POU class 2 homeobox 3 (*POU2F3*) or yes-associated protein (*YAP*) respectively (McKoll 2017, Huang 2018, Rudin 2019).

Functionally, *ASCL1* and *NEUROD1* regulate distinct gene expression profiles and are associated with different SCLC driver genes (Borromeo 2016). For example, *MYC* overexpression has been shown to drive SCLC to a *NEUROD1* high variant phenotype in a mouse model of SCLC while high levels of *MYCL* and *MYCN* expression are more commonly seen in *ASCL1* high classic SCLC (Mollaoglu 2017).

As SCLC is largely a disease of smokers, SCLC tumors, regardless of subtype, typically display a high degree of somatic mutation. Inactivating mutations in *RB1* and *TP53* are present in nearly 100% of cases. Furthermore, a significant portion of tumors also exhibit inactivating mutations in chromatin regulators such as *CREBBP*, *EP300*, *KMT2D*, and *PBRM1* (Peifer 2012, Rudin 2012, George 2015, Iwakawa 2015, Augert 2017). Other common genetic alterations include inactivating mutations in *PTEN* and *NOTCH* pathway components as well as amplification of MYC family basic helix loop helix transcription factors including *MYC*, *MYCN*, and *MYCL* (Peifer 2012, Rudin 2012, George 2015, Iwakawa 2015, Augert 2017).

One major barrier to understanding chemoresistant SCLC has been the dearth of genomically characterized tumors from chemotherapy treated patients. As tumors are not typically resected during the course of clinical care, most large genomic studies in SCLC have focused on untreated patients. While genomically characterized chemotherapy treated tumor samples are rare, a recent analysis of 30 chemotherapy treated, relapsed SCLC patients implicated WNT pathway alterations in chemoresistance (Wagner 2018). Furthermore, a recent study in which SCLC PDX models were treated for an extended period of time with chemotherapy found that loss of *SLFN11* was associated with the development of chemoresistance in a subset of

models (Gardner 2017). Beyond these studies, little else is known about key drivers of SCLC chemoresistance. Despite the relative paucity of available chemotherapy treated SCLC patient samples, observations of a ~4-fold increased rate of high-level *MYC*, *MYCN*, or *MYCL* amplification in cell lines derived from chemotherapy treated vs. chemonaive patients indirectly implicate MYC family amplification (Johnson 1987). Additionally, a MYC transcriptional signature has previously been associated with chemoresistance in human SCLC PDX models derived from chemonaive vs. treated patients (Drapkin 2018). Despite these hints that MYC family activation could contribute to SCLC chemoresistance, this notion has yet to be demonstrated using robust in vivo models. In Chapter 2, we highlight the use of multiple models of SCLC to demonstrate that the MYC family members, *MYCN* and *MYCL* confer chemoresistance.

### 1.3 Pre-clinical Models of Small Cell Lung Cancer

In the early days of SCLC research, the predominant models used to study this disease were immortalized cell lines derived from human SCLC patients, either from primary tumors, distal metastases, or pleural effusions (Gazdar 1980, Carney 1985, Brennan 1991, Phelps 1996). While useful for studying SCLC in some contexts, SCLC derived cell lines are limited in their capacity to recapitulate features of human disease such as hypoxia and altered metabolism (Han 2020). In recent decades, many advances have been made in the development of mouse model systems of SCLC. The first genetically engineered mouse (GEM) model of SCLC was created by introduction of floxed alleles of both *Rb1* and *Trp53*, key tumor suppressors that are nearly universal inactivated in human SCLC. Following delivery of adenovirus expressing Cre recombinase into the lungs via intratracheal intubation, this model (herein referred to as *RP*) develops lung

tumors that are histologically similar to human SCLC (Meuwissen 2003). Over the years, this baseline *RP* model has been expanded upon to generate GEM models that incorporate additional floxed alleles of genes of interest in SCLC, including *Rbl2*, *Nfib*, *Pten*, and *Crebbp* among others (DuPage 2009, Schaffer 2010, Dooley 2011, Cui 2014, Jia 2018). Models have also been generated that incorporate Cre-activated transgenes onto the *RP* background for the study of oncogenes such as *Myc* (Mollaoglu 2017). In our study, we made use of 2 such GEM models in which the introduction of adenovirus expressing Cre recombinase via intratracheal intubation leads to the development of SCLC tumors that exhibit overexpression of either *MYCL* (herein *RPMYCL*) or *MYCN* (herein *RPMYCN*) in addition to loss of *Rb1* and *Trp53* (Huijbers 2014, Kim 2016).

One of the most important developments for the study of SCLC in recent years has been the advent of patient derived xenograft (PDX) models generated from SCLC patients. In SCLC, PDX models can be generated by direct implantation of patient tumor tissue into the flank of an immunocompromised mouse, most commonly a NOD-SCID gamma (NSG) mouse (Daniel 2009). Alternatively, PDX models can be generated by isolating circulating tumor cells from patient blood samples and propagating those cells as tumors in NSG mice (Hodgkinson 2014). Over the years, our lab and others have generated dozens of PDX models derived from SCLC patients at various stages of treatment ranging from those who have never received any chemotherapy to those who have had relapse of chemoresistant disease (Daniel 2009, Hodgkinson 2014, Drapkin 2018, Augert 2019). A major advantage of PDX models is that they tend to recapitulate many features of the patient tumors that they were derived from (Drapkin 2018), allowing for comprehensive studies of SCLC drivers. In our study, we made use of 2

such PDX models, FHSC14 and FHSC23, that were derived in house from chemonaive patients. Both of these models strongly regress upon treatment with platinum-based chemotherapy, making them ideal systems in which to study potential drivers of SCLC chemoresistance (Augert 2019).

### 1.4 CRISPR-Cas9 Screens in Cancer

The recent development of clustered regularly interspaced short palindromic repeats (CRISPR)-Cas9 gene editing technology has been heralded as one of the most important advances in modern molecular biology. In brief, the most widely utilized CRISPR-Cas9 gene editing system involves the use of Cas9, a bacterial endonuclease that cleaves DNA to induce double stranded DNA breaks (Cong 2013). Eukaryotic cells typically repair these breaks via non-homologous end joining, which often results in the introduction of insertion or deletion (indel) mutations. The introduction of indels can result in loss of function if they occur in the coding region of a gene. Cas9 can be directed to specific sites in the genome using a single-guide RNA (sgRNA), a construct consisting of a fusion between a CRISPR RNA (crRNA) and a trans-activating crRNA (tracrRNA) (Jinek 2012, Cong 2013, Mali 2013). By designing custom sgRNAs targeting specific genes, the CRISPR-Cas9 system can be utilized for precise, highly efficient knockout of genes of interest (Cong 2013, Mali 2013, Hsu 2014). In addition to its specificity, a major advantage of the CRISPR-Cas9 system as compared to earlier modes of gene editing such as shRNA, is that CRISPR-Cas9 editing generally results in complete gene knockout rather than incomplete knockdown of a target (Evers 2016).

In recent years, the CRISPR-Cas9 system has been adapted for use in genome-wide functional screens. This technique involves the use of a (usually) lentiviral system

containing Cas9 cDNA along with a library of sgRNAs each designed against the coding region of a given gene (Shalem 2015). For example, the widely available Human GeCKO Lentiviral sgRNA Library v2 expresses a pool of 123,411 sgRNAs targeting 19,050 genes, with each gene having a corresponding 4-6 sgRNAs (Sanjana 2014). In one of the basic formats of a CRISPR-Cas9 screen, a cell line is infected using lentivirus containing an sgRNA library. A subset of cells is then collected as an early timepoint (referred to as a P0) and the remainder of infected cells are passaged for a given number of population doublings. Genomic DNA from both cell populations is then sequenced to determine the relative abundance of specific sgRNAs between the P0 and endpoint samples. In this setup, negative enrichment of sgRNAs in the end population signifies potential essential genes while positive enrichment of sgRNAs signifies genes whose loss confers a pro-survival effect (Shalem 2014, Wang 2014). This baseline setup can be expanded upon to identify genes that exhibit synthetic lethal interactions in cells harboring a specific genetic mutation (Wang 2017) or genes that play an important role in regulating response to specific pharmacologic inhibitors (Ruiz 2016, Hou 2017). To date numerous studies have extensively demonstrated the use of CRISPR-Cas9 in human cell lines derived from many cancer types (Sanchez-Rivera 2015, Chow 2018). For example, a recent CRISPR-Cas9 screen using cell lines derived from an autochthonous mouse model of SCLC identified the enzyme DHODH as a potential therapeutic target (Li 2019).

As noted earlier, there are significant limitations to the use of cell lines in culture for investigating genes that modulate response to treatment in different cancers (Han 2020). As such, CRISPR-Cas9 technology has been further adapted for use in in vivo

CRISPR-Cas9 functional screens. One version of an in vivo CRISPR-Cas9 screen involves infecting cancer cell lines or PDX models with lentivirus containing an sgRNA library system. The infected population is then injected into a cohort of immunocompromised mice to allow for flank tumor development. Tumors from different groups of mice can then be harvested and analyzed to determine the effects of different treatments on sgRNA abundance or to assess levels of specific sgRNAs in primary tumor and metastases populations (Chen 2015, Manguso 2017). Another approach to in vivo CRISPR-Cas9 screens involves orthotopic injection of a CRISPR-Cas9 sgRNA library vector system into a specific site to allow for endogenous tumor development. In a recently published study, the authors used intratracheal intubation to deliver an adenoviral vector containing a CRISPR-Cas9 sgRNA library system to a cohort of RP mice and later assessed guide abundance in the resulting SCLC tumors (Ng 2020). The development of CRISPR-Cas9 screen technology along with the advent of robust PDX models presents a unique opportunity to thoroughly interrogate the development of resistance to chemotherapy in SCLC. In Chapter 3 of this study, we performed in vivo CRISPR-Cas9 functional screens in a chemosensitive PDX model to identify potential drivers of SCLC chemoresistance.

## CHAPTER 2: *MYCN* and *MYCL* Drive Chemoresistance in Small Cell Lung Cancer

### 2.1 *MYCN/L* Overexpression Drives Chemoresistance in a Genetically Engineered Mouse Model of SCLC

Based on more frequent amplifications of MYC family members in cell lines derived from chemoresistant SCLC patients, we hypothesized that *MYCN* or *MYCL* overexpression may confer chemoresistance (Johnson 1987). To test this hypothesis,

we first made use of the *RPMYCN* and *RPMYCL* GEM models. We used magnetic resonance imaging (MRI) to monitor *RP, RPMYCN, and RPMYCL* mice for the development of lung tumors. Once mice exhibited significant tumor burden, we treated tumor bearing mice with either saline or cisplatin-etoposide (cis-eto) chemotherapy for 21 days (3 weekly cycles of treatment). We then used sequential MRI scans at days 14 and 21 to calculate changes in tumor volume relative to baseline. In doing so, we found that while *RP* mice exhibited a cytostatic response to chemotherapy, both *RPMYCN* and *RPMYCL* tumors continued to grow through treatment at a rate comparable to saline treated tumors at both 14 and 21 days (Fig. 2.1A-C). To assess the functional effects of *MYCN* and *MYCL* overexpression on acute response to chemotherapy, we treated another cohort of *RP, RPMYCN*, and *RPMYCL* mice with a single cycle of either saline or cis-eto and collected lung tumors 72 hours post treatment. Using TUNEL staining to assess levels of apoptosis, we found that while *RP* tumors exhibited increased apoptosis in response to cis-eto treatment, neither *RPMYCN* nor *RPMYCL* tumors exhibited a significant increase in apoptosis following chemotherapy (Fig. 2.1D, E). Conversely, using phosphor-H3 (pH3) staining to assess proliferation, we found that while *RP* tumors exhibited a marked decrease in proliferation upon treatment with cis-eto, neither *RPMYCN* nor *RPMYCL* tumors exhibited decreased proliferation following chemotherapy (Fig. 2.1D, F). Taken together, these data show that overexpression of either *MYCN* or *MYCL* is sufficient to abrogate the response to cis-eto in an established GEM model of SCLC.

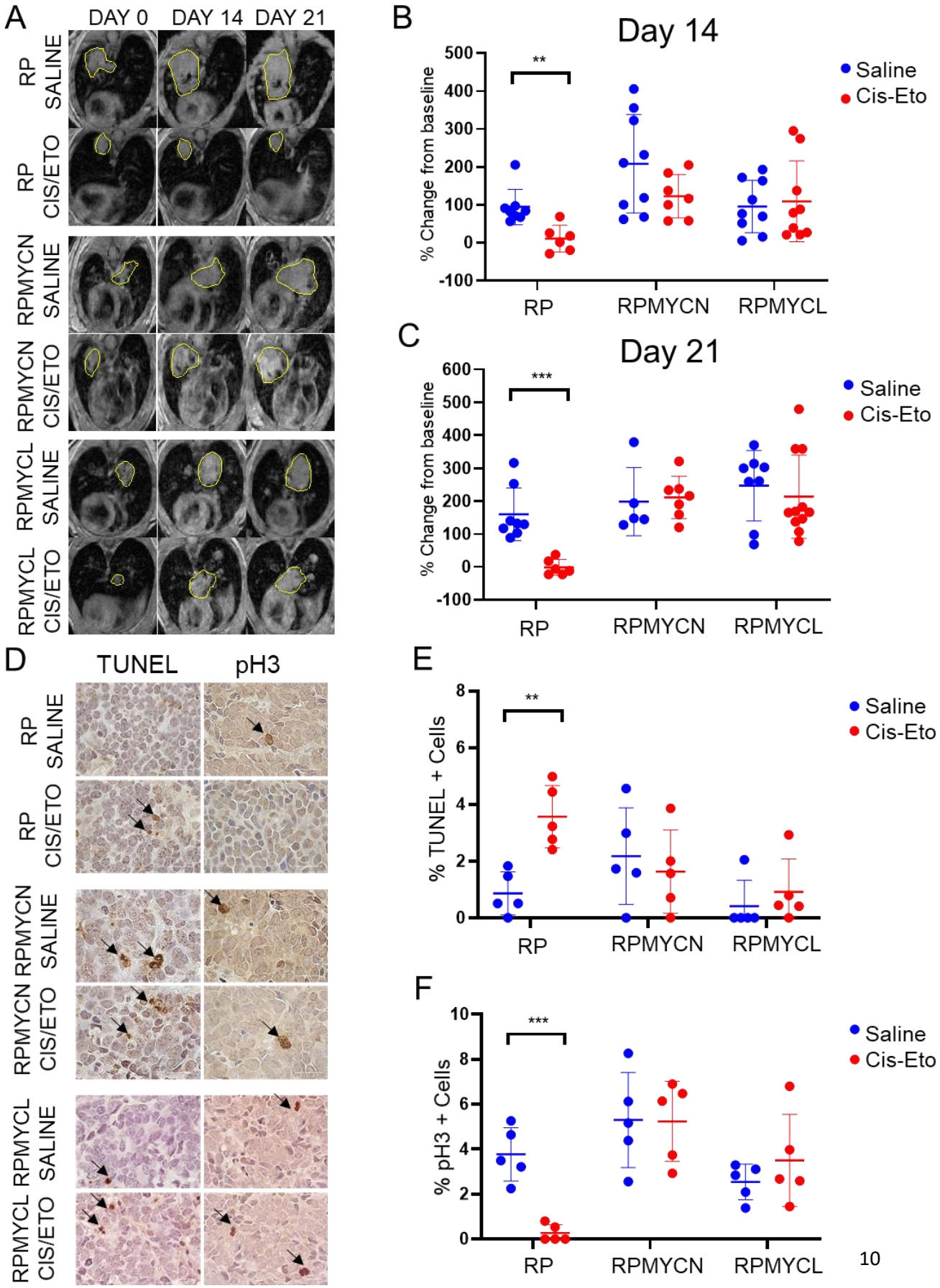
A
DAY 0
DAY 14
DAY 21
RP SALINE
RP CIS/ETO
RPMYCN SALINE
RPMYCN CIS/ETO
RPMYCL SALINE
RPMYCL CIS/ETO
B
Day 14
% Change from baseline
500
400
300
200
100
0
-100
**
RP
RPMYCN
RPMYCL
Saline
Cis-Eto
C
Day 21
% Change from baseline
600
500
400
300
200
100
0
-100
***
RP
RPMYCN
RPMYCL
Saline
Cis-Eto
D
TUNEL
pH3
RP SALINE
RP CIS/ETO
RPMYCN SALINE
RPMYCN CIS/ETO
RPMYCL SALINE
RPMYCL CIS/ETO
E
% TUNEL + Cells
8
6
4
2
0
**
RP
RPMYCN
RPMYCL
Saline
Cis-Eto
F
% pH3 + Cells
10
8
6
4
2
0
***
RP
RPMYCN
RPMYCL
Saline
Cis-Eto

**Figure 2.1: *MYCN* and *MYCL* drive chemoresistance in an SCLC mouse model** (A) Representative MRI of *RP*, *RPMYCN*, and *RPMYCL* lungs at days 0, 14, and 21 of cis-eto treatment. Tumors are circled in yellow. (B) Quantification of % change in tumor volume between days 0 and 14 of treatment. Data are means ± SEM (*RP* SALINE: n=8, *RP* CIS-ETO: n=6, *RPMYCN* SALINE: n=9, *RPMYCN* CIS-ETO: n=7, *RPMYCL* SALINE: n=9, *RPMYCL* CIS-ETO: n=9). Significance was determined using two-tailed unpaired Student's t test. **p<0.01 as determined by student's t test. (C) Quantification of % change in tumor volume between days 0 and 21 of treatment. Data are means ± SEM (*RP* SALINE: n=8, *RP* CIS-ETO: n=6, *RPMYCN* SALINE: n=5, *RPMYCN* CIS-ETO: n=7, *RPMYCL* SALINE: n=8, *RPMYCL* CIS-ETO: n=11). Significance was determined using two-tailed unpaired Student's t test. ***p<0.001. (D) Representative immunohistochemistry images for pH3 and TUNEL staining in a parallel cohort comparing *RP*, *RPMYCN*, and *RPMYCL* tumors at a 3 day timepoint of treatment with either saline or cis-eto. Scale bar = 20μm (E) Quantification of % TUNEL positive cells. Data are means ± SEM (n=5 in all groups). Significance was determined using two-tailed unpaired Student's t test. **p<0.01. (F) Quantification of % pH3 positive cells. Data are means ± SEM. (n=5 in all groups). Significance was determined using two-tailed unpaired Student's t test. ***p<0.001.

## 2.2 *MYCN/L* Overexpression Drives Chemoresistance in Patient Derived Xenograft Models of SCLC

While GEM models are a valuable tool for studying SCLC, they exhibit characteristics which render them suboptimal for investigating SCLC chemoresistance. Most

importantly, the baseline *RP* autochthonous model typically exhibits cytostatic responses to cis-eto treatment (Fig. 2.1A-C), with only rare tumor regressions. This is in stark contrast to SCLC patients where the predominant response to chemotherapy is robust tumor regression followed by relapse months later (Rossi 2012). In order to better model the cytoreductive responses to cis-eto treatment seen in most SCLC patients, we turned to two SCLC PDX models, FHSC14 and FHSC23, that we previously generated from chemonaive patients (Augert 2019). Both of these PDX models were derived from classic *ASCL1*-high SCLC, are highly chemosensitive, and exhibit flank tumor regressions with 3 weeks of cis-eto treatment. FHSC14 and FHSC23 PDX tumors growing in NSG mice were harvested, dissociated, and infected ex vivo with high titer lentivirus expressing either a *MYCN* cDNA, *MYCL* cDNA, or an empty control. Within 16 hours of tumor extraction and addition of lentivirus, the infected cells were re-injected into the flanks of NSG mice. Once flank tumors reached a volume of 150mm$^3$ as measured by digital calipers, we treated the mice with 3 weekly cycles of either saline or cis-eto and measured tumor volume over the course of 21 days and then collected the remaining tumor tissues for molecular analyses. We observed that both FHSC14 and FHSC23 empty vector infected tumors strongly regressed upon treatment with cis-eto (Fig. 2.2A, B, 2.3A, B). In contrast, in both the FHSC14 and FHSC23 models, tumors derived from *MYCN*-overexpressing and *MYCL*-overexpressing cells grew robustly throughout the cis-eto treatment period (Fig. 2.2A, B, 2.3A, B). For both models, we validated the overexpression of N-MYC and L-MYC respectively using immunoblotting (Fig. 2.2C, D, 2.3C, D). As such, our data definitively show that overexpression of a single gene, either *MYCN* or *MYCL*, is sufficient to switch

two highly chemosensitive models of SCLC to become resistant. These results demonstrate the first known instances where gene overexpression can directly drive SCLC chemoresistance. To assess the short term response to chemotherapy in *MYCL*- or *MYCN*-overexpressing PDX models, we set up an additional cohort of NSG mice as described above in which we treated with only a single cycle of either saline or cis-eto and collected tumors 72 hours post treatment. Using TUNEL staining to assess levels of apoptosis, we found that while FHSC14 and FHSC23 empty vector tumors exhibited increased apoptosis in response to cis-eto treatment, neither *MYCN*-overexpressing nor *MYCL*-overexpressing tumors in either model exhibited a significant increase in apoptosis following chemotherapy (Fig. 2.2E, F, 2.3E, F). Conversely, using pH3 staining to assess proliferation, we observed that FHSC14 and FHSC23 empty vector tumors exhibited a marked decrease in proliferation upon treatment with cis-eto, while *MYCN*- or *MYCL*-overexpressing tumors showed no signs of decreased proliferation following chemotherapy (Fig. 2.2G, H, 2.3G, H). As in the GEM model, these data clearly demonstrate that *MYCN* or *MYCL* overexpression alone is sufficient to abrogate the response to chemotherapy in otherwise highly chemosensitive models.

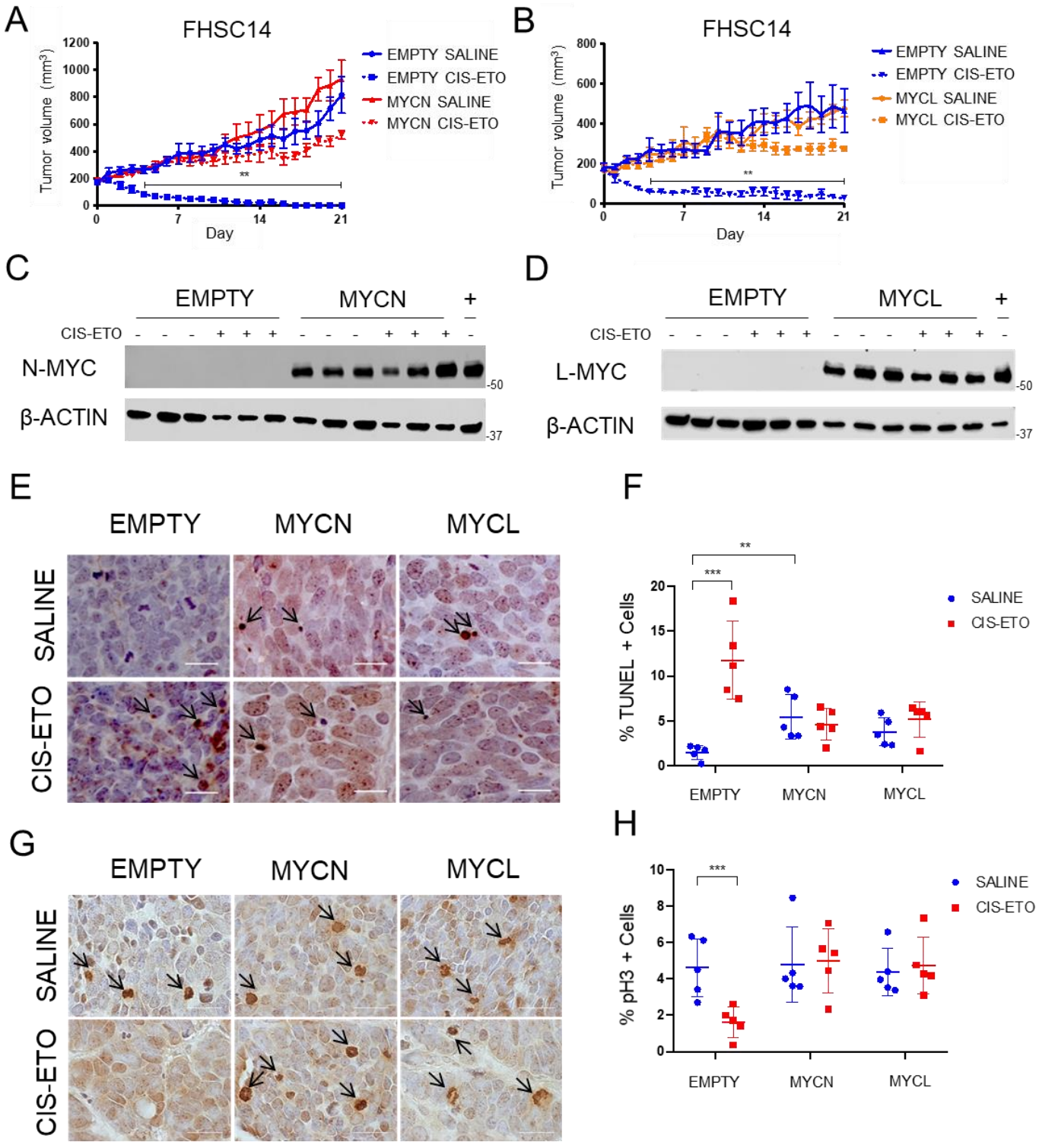


**Figure 2.2: *MYCN* or *MYCL* overexpression abrogates chemotherapy response in the FHSC14 model** (A) Graph showing flank tumor volumes of empty control vs. *MYCN*

overexpressing FHSC14 PDX tumors over 21 days of treatment with either saline or 3 cycles of cis-eto. Data are means ± SEM (n=5 in all groups). Significance was determined using a mixed model two-way ANOVA followed by a posthoc Tukey's multiple comparisons test. For each group, significance is presented relative to the respective saline condition. **p<0.01 (B) Graph showing flank tumor volumes of empty control vs. *MYCL*-overexpressing FHSC14 PDX tumors over 21 days of treatment with either saline or 3 cycles of cis-eto. Data are means ± SEM (n=5 in all groups). Significance was determined using a mixed model two-way ANOVA followed by a posthoc Tukey's multiple comparisons test. For each group, significance is presented relative to the respective saline condition. **p<0.01 (C) Immunoblot showing successful *MYCN* overexpression in the FHSC14 PDX model. Lysate from a PDX model containing a *MYCN* amplification was used as a positive control in the rightmost lane. β-ACTIN was used as a loading control. (D) Immunoblot showing successful *MYCL* overexpression in the FHSC14 PDX model. Lysate from a cell line derived from an *RP* tumor containing a *MYCL* amplification was used as a positive control in the rightmost lane. β-ACTIN was used as a loading control. (E) Representative immunohistochemistry images for TUNEL staining in a parallel cohort comparing FHSC14 empty, *MYCN* overexpressing, and *MYCL* overexpressing tumors at a 3 day timepoint after treatment with either saline or cis-eto. Scale bar = 20μm (F) Quantification of % TUNEL positive cells. Data are means ± SEM (n=5 in all groups). Significance was determined using two-tailed unpaired Student's t test. *p<0.05, **p<0.01. (G) Representative immunohistochemistry images for pH3 staining in a parallel cohort comparing FHSC14 empty, *MYCN* overexpressing, and *MYCL* overexpressing tumors at a 3 day timepoint after treatment with either saline or cis-eto. Scale bar = 20μm

(H) Quantification of % pH3 positive cells. Data are means ± SEM. (n=5 in all groups). Significance was determined using two-tailed unpaired Student's t test. **p<0.01.

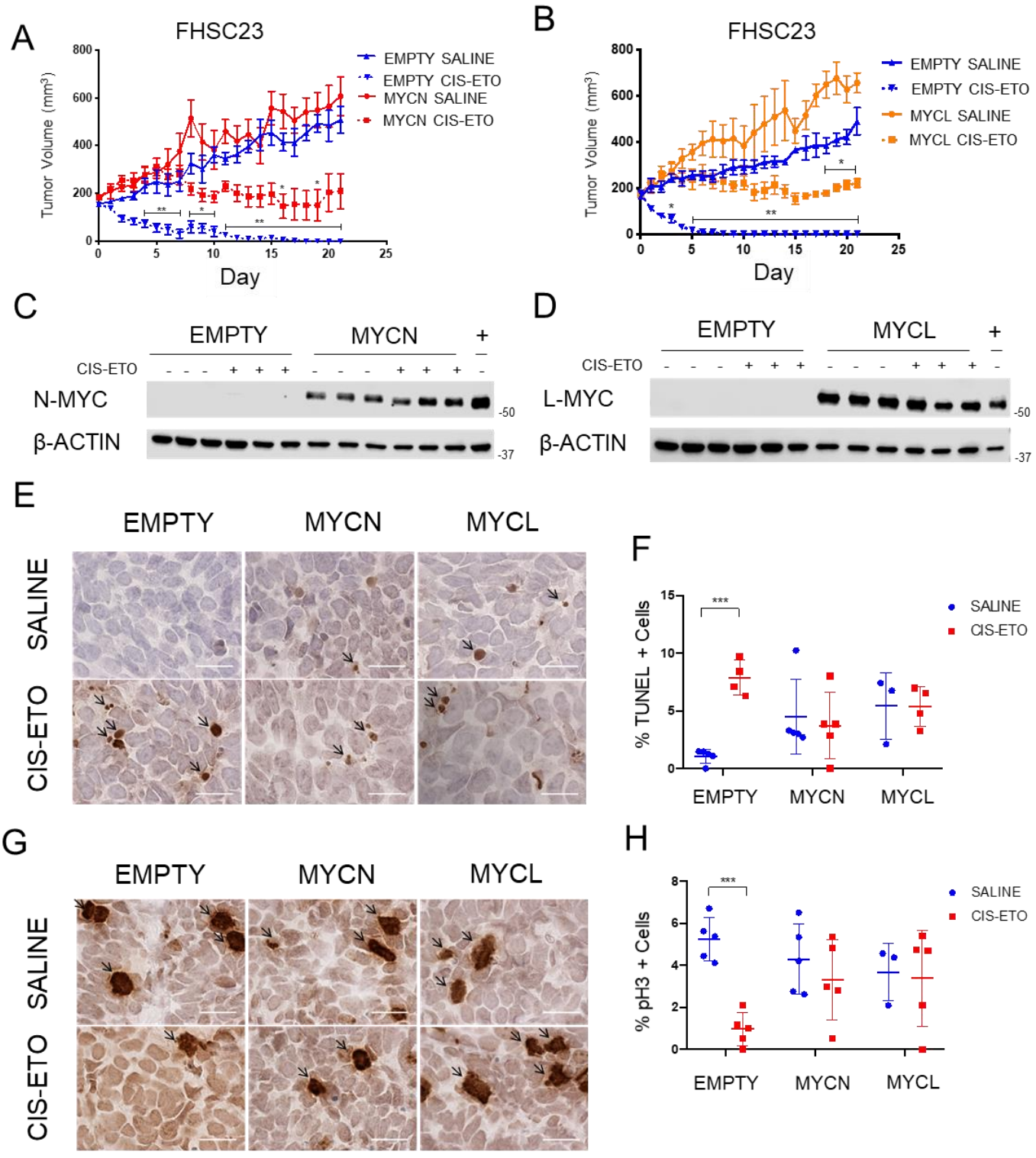


**Figure 2.3: *MYCN* or *MYCL* overexpression abrogates chemotherapy response in the FHSC23 model** (A) Graph showing flank tumor volumes of empty control vs. *MYCN*

overexpressing FHSC23 PDX tumors over 21 days of treatment with either saline or 3 cycles of cis-eto. Data are means ± SEM (n=5 in all groups). Significance was determined using a mixed model two-way ANOVA followed by a posthoc Tukey's multiple comparisons test. For each group, significance is presented relative to the respective saline condition. *p<0.05, **p<0.01 (B) Graph showing flank tumor volumes of empty control vs. *MYCL* overexpressing FHSC23 PDX tumors over 21 days of treatment with either saline or 3 cycles of cis-eto. Data are means ± SEM (n=5 in all groups). Significance was determined using a mixed model two-way ANOVA followed by a posthoc Tukey's multiple comparisons test. For each group, significance is presented relative to the respective saline condition. *p<0.05, **p<0.01 (C) Immunoblot showing successful N-MYC overexpression in the FHSC23 PDX model. Lysate from a PDX model expressing *MYCN* was used as a positive control in the rightmost lane. β-ACTIN was used as a loading control. (D) Immunoblot showing successful L-MYC overexpression in the FHSC23 PDX model. Lysate from a cell line derived from an *RP* tumor containing a *MYCL* amplification was used as a positive control in the rightmost lane. β-ACTIN was used as a loading control. (E) Representative immunohistochemistry images for TUNEL staining in a parallel cohort comparing FHSC23 empty, *MYCN* overexpressing, and *MYCL* overexpressing tumors at a 3 day timepoint after treatment with either saline or cis-eto. Scale bar = 20μm (F) Quantification of % TUNEL positive cells. Data are means ± SEM (n=5 in all groups). Significance was determined using two-tailed unpaired Student's t test. **p<0.01, ***p<0.001 (G) Representative immunohistochemistry images for pH3 staining in a parallel cohort comparing FHSC23 empty, *MYCN* overexpressing, and *MYCL* overexpressing tumors at a 3 day timepoint after treatment with either saline or

cis-eto. Scale bar = 20μm (H) Quantification of % pH3 positive cells. Data are means ± SEM. (n=5 in all groups). Significance was determined using two-tailed unpaired Student's t test. ***p<0.001.

### 2.3 USP7 Inhibition Restores Chemosensitivity in *MYCN*-Overexpressing SCLC

Having shown that MYC family members can drive chemoresistance in SCLC, we next sought to find strategies to therapeutically target *MYCN*-overexpressing SCLC. To uncover unique vulnerabilities in *MYCN*-driven SCLC, we made use of genome-scale CRISPR-Cas9 small guide (sgRNA) inactivation screens that had been previously run in the lab using cell lines derived from *RP* and *RPMYCN* GEMM tumors respectively. In those screens, we infected 3 *RP* and 3 *RPMYCN* derived cell lines with lentivirus containing the Murine GeCKO Lentiviral sgRNA Library v2 vector system, which expresses a pool of 130,209 sgRNAs targeting 20,611 genes (Sanjana 2014). Following infection, cells were subjected to puromycin selection after which a portion of cells from each cell line was collected as an initial timepoint (P0). The remaining cells were grown out in culture for 12 population doublings and then collected (P12). Using deep sequencing, we compared the abundance of sgRNAs in the P0 and P12 populations for each *RP* and *RPMYCN* cell line (Fig. 2.4A). For each gene, we generated a "CRISPR score", defined as: $\log_2$ (sgRNA abundance at P12/sgRNA abundance at P0) averaged across all sgRNAs targeting a given gene (6 sgRNAs per gene in most cases) (Wang 2015). Furthermore, we employed MAGeCK-MLE analysis to determine which sgRNAs were preferentially depleted in *RPMYCN* cell lines as compared to *RP* cell lines (Li 2014). Our analysis revealed that sgRNAs targeting druggable genes such as *WEE1*,

*BRD2*, and *USP7* were preferentially depleted after 12 population doublings in the *RPMYCN* cell lines as compared to the *RP* cell lines (Fig. 2.4B,C). We were particularly interested in *USP7* which encodes a deubiquitinase that directly de-ubiquitinates N-MYC, resulting in increased protein stability (Tavana 2016). Given this, we hypothesized that USP7 could be a viable synthetic lethal target for *MYCN*-driven SCLC. To test this, we made use of a novel inhibitor of USP7, herein referred to as USP7i, procured from RAPT Therapeutics. This compound potently inhibits USP7 and is from a series that has shown high selectivity against a panel of other deubiquitinases. Consistent with our genetic screen results, we found that *RPMYCN* cell lines exhibited increased sensitivity to treatment with USP7i as compared to *RP* cell lines (Fig. 2.4D, 2.5A,B). Furthermore, analysis by immunoblotting revealed that treatment of *RPMYCN* cell lines with USP7i led to decreased levels of N-MYC protein as well as increased levels of cleaved caspase 3, indicative of apoptosis (Fig. 2.4E). As such, USP7 shows promise as a druggable synthetic vulnerability in *MYCN*-driven SCLC.

Having found that pharmacologic inhibition of USP7 can selectively target *MYCN*-driven SCLC, we next sought to determine whether USP7 inhibition could restore chemosensitivity in *MYCN*-overexpressing, chemoresistant PDX models. To improve upon the overexpression model system described earlier, we switched to a multi-step system in which we sorted productively infected cells following expansion in vivo, thereby ensuring complete lentiviral transduction before propagating for therapeutic experiments. We infected the chemosensitive FHSC14 model with lentivirus containing either a *MYCN* cDNA-IRES-ZsGreen vector, a *MYCL* cDNA-IRES-ZsGreen vector, or an empty control vector and then injected the cells into the flanks of NSG mice as

described earlier. Once flank tumors developed, we harvested the tumors, dissociated cells, and used fluorescence activated cell sorting (FACS) to obtain pure populations of ZsGreen-positive *MYCN*-overexpressing, *MYCL*-overexpressing, or empty vector control FHSC14 cells. We then injected these populations into the flanks of NSG mice to allow for tumor development. Once flank tumors formed, we validated pure populations of infected cells by FACS (Fig. 2.6) and re-injected cells into a cohort of NSG mice for therapeutic studies. Once tumors reached a volume of 150mm$^3$, we treated the mice with either saline, cis-eto, USP7i (100mg/kg), or a combination therapy of USP7i (100mg/kg) alongside standard cis-eto (USP7i-cis-eto) and measured flank tumor volumes over the course of 14 days. In doing so, we found that while cis-eto caused near complete tumor regression in empty vector control tumors, treatment with USP7i alone had no effect on tumor growth (Fig. 2.7A,B). In the *MYCL*-overexpressing tumors, neither cis-eto nor USP7i alone or in combination had any significant effect on tumor volume (Fig. 2.7B). However, in the *MYCN*-overexpressing tumors, while cis-eto alone did not slow tumor growth, as expected given *MYCN*-driven chemoresistance, we found that combination USP7i-cis-eto treatment resulted in complete tumor regression in a manner similar to the empty vector control tumors under cis-eto treatment (Fig. 2.7A). Due to concerns related to mouse weight loss in response to 100mg/kg of USP7i, we set up a validation cohort of FHSC14 *MYCN*-overexpressing and empty vector mice using a reduced dose of USP7i (50mg/kg) which was better tolerated (Fig. 2.8A, B). This experiment was run for 21 days with all cis-eto and USP7i treatments administered in their respective groups during weeks one and three. Once again, we observed that *MYCN*-overexpressing tumors were resistant to cis-eto alone but strongly regressed

upon treatment with USP7i-cis-eto (Fig. 2.7C). These data conclusively show that inhibition of USP7 can re-sensitize *MYCN*-overexpressing SCLC to cytotoxic chemotherapy. To assess the acute effects of the different treatment groups, we repeated this experiment but treated the mice with only a single cycle of cis-eto and/or USP7i for 7 days after which tumors were collected. In doing so we found that treatment with USP7i dramatically reduced levels of N-MYC in *MYCN*-overexpressing tumors (Fig. 2.7D). Furthermore, immunostaining for TUNEL and pH3 again confirmed that *MYCN*-overexpressing tumors are resistant to the increased apoptosis and decreased proliferation normally induced by cis-eto in empty vector tumors. Remarkably, *MYCN*-overexpressing tumors in the USP7i-cis-eto treatment group exhibited reduced proliferation and increased apoptosis consistent with the strong tumor regression observed with combined USP7i inhibition and chemotherapy in the *MYCN*-overexpressing model (Fig. 2.7E-H). Taken together, these data demonstrate that USP7 inhibition is a viable therapeutic strategy that could potentially be used clinically to treat recalcitrant, chemoresistant SCLC.

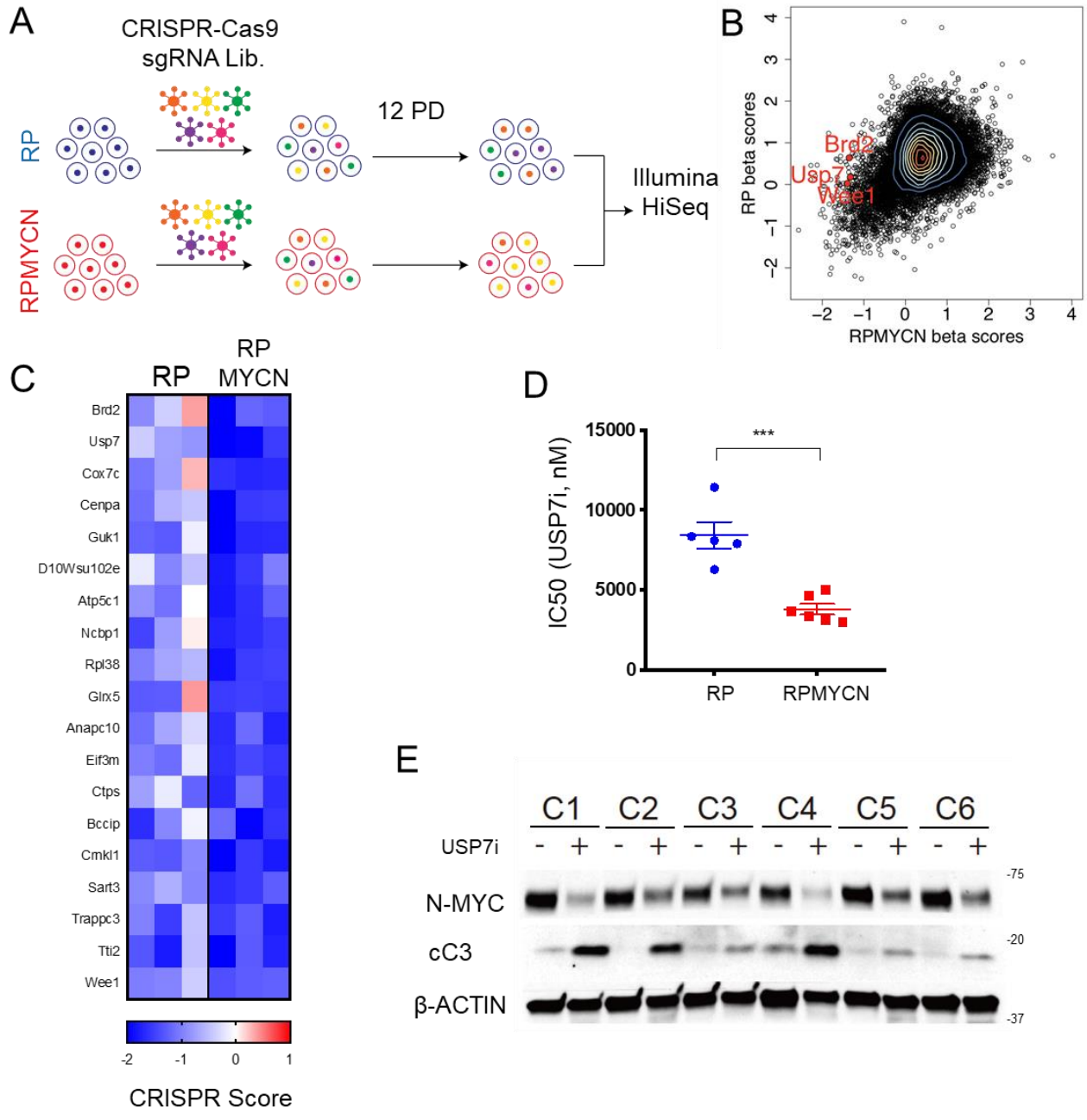


**Figure 2.4: CRISPR inactivation screens reveal *USP7* as a *MYCN* synthetic vulnerability** (A) Schematic outlining the strategy used in a genome scale CRISPR-Cas9 sgRNA screen comparing cell lines derived from *RP* and *RPMYCN* tumors (n=3 cell lines in both groups). (B) Contour plot comparing MAGeCK analysis generated β-scores for

*RP* derived lines (y-axis) vs. *RPMYCN* derived lines (x-axis). Each data point (shown as a black circle) represents a single gene in the sgRNA library. A positive β-score indicates that guide RNAs targeting a given gene are present in a higher proportion after 12 population doublings while a negative β-score indicates that guide RNAs targeting a given gene are present in a lower proportion after 12 population doublings. A selection of known druggable targets that exhibit a significantly lower beta score in *RPMYCN* lines as compared to *RP* lines are highlighted in red. Genes with fewer than 5 associated sgRNAs were omitted. (C) Heatmap showing CRISPR scores of 19 selected genes for each *RP* and *RPMYCN* derived cell line. Genes were selected based on statistical significance from MAGECK analyses and ordered based on greatest difference in *RPMYCN* and *RP* CRISPR scores. (D) Comparison of IC50 for USP7i between *RP* and *RPMYCN* derived cell lines. Data are means ± SEM from n=5 cell lines (*RP*) and n=6 cell lines (*RPMYCN*). Data from each individual cell line is from 3 biological replicates each consisting of 3 technical replicates. Significance was determined using two-tailed unpaired Student's t test. ***$p<0.001$. (E) Immunoblot comparing levels of N-MYC and cleaved caspase 3 in 6 *RPMYCN* derived cell lines (C1-6) either with or without USP7i treatment. β-Actin was used as a loading control.

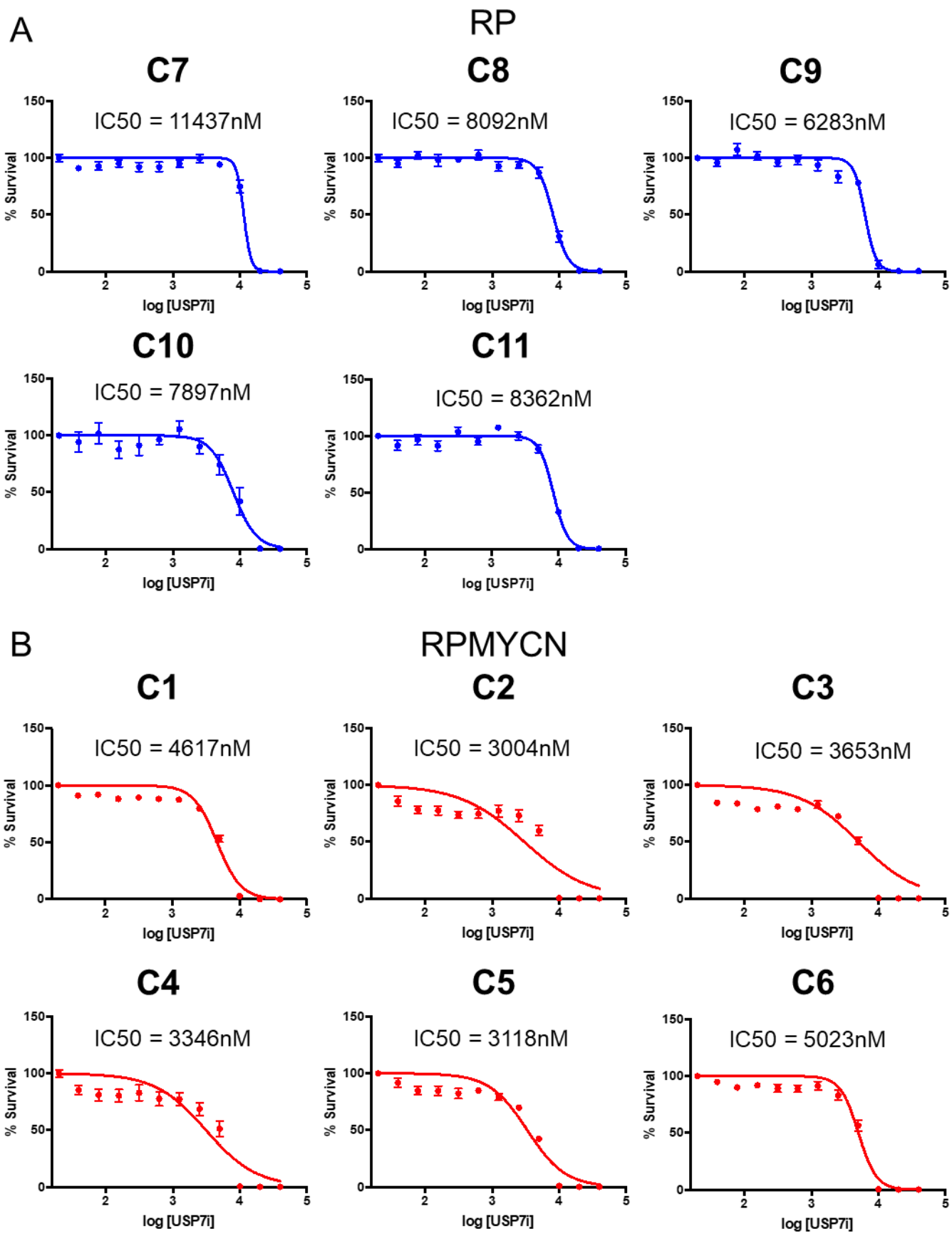
A
RP
C7
IC50 = 11437nM
C8
IC50 = 8092nM
C9
IC50 = 6283nM
C10
IC50 = 7897nM
C11
IC50 = 8362nM
B
RPMYCN
C1
IC50 = 4617nM
C2
IC50 = 3004nM
C3
IC50 = 3653nM
C4
IC50 = 3346nM
C5
IC50 = 3118nM
C6
IC50 = 5023nM
% Survival
log [USP7i]

**Figure 2.5: *MYCN*-overexpressing cell lines exhibit increased USP7i sensitivity** Dose response curves and IC50 values of 5 *RP* derived cell lines (C7-11) treated for 72 hours with USP7i. Data are means ± SEM (n=3 biological replicates with 3 technical replicates each). (B) Dose response curves and IC50 values of 6 *RPMYCN* derived cell lines (C1-6) treated for 72 hours with USP7i. Data are means ± SEM (n=3 biological replicates with 3 technical replicates each).

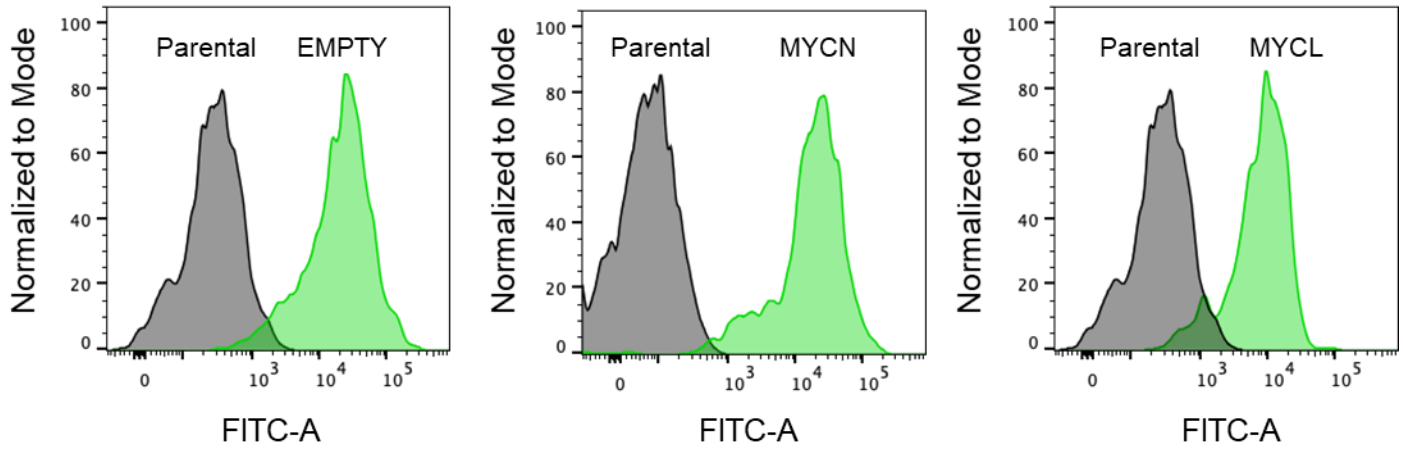


**Figure 2.6: Generation of *MYCN* and *MYCL* overexpressing PDX models** (A) Flow analysis of FHSC14 *MYCN* overexpressing, *MYCL* overexpressing, or EMPTY control tumors generated from PDX models that were re-injected into NSG mice following sorting for ZsGreen positive cells. Histograms show normalized counts of cells on the y axis and intensity of FITC class expression on the x axis.

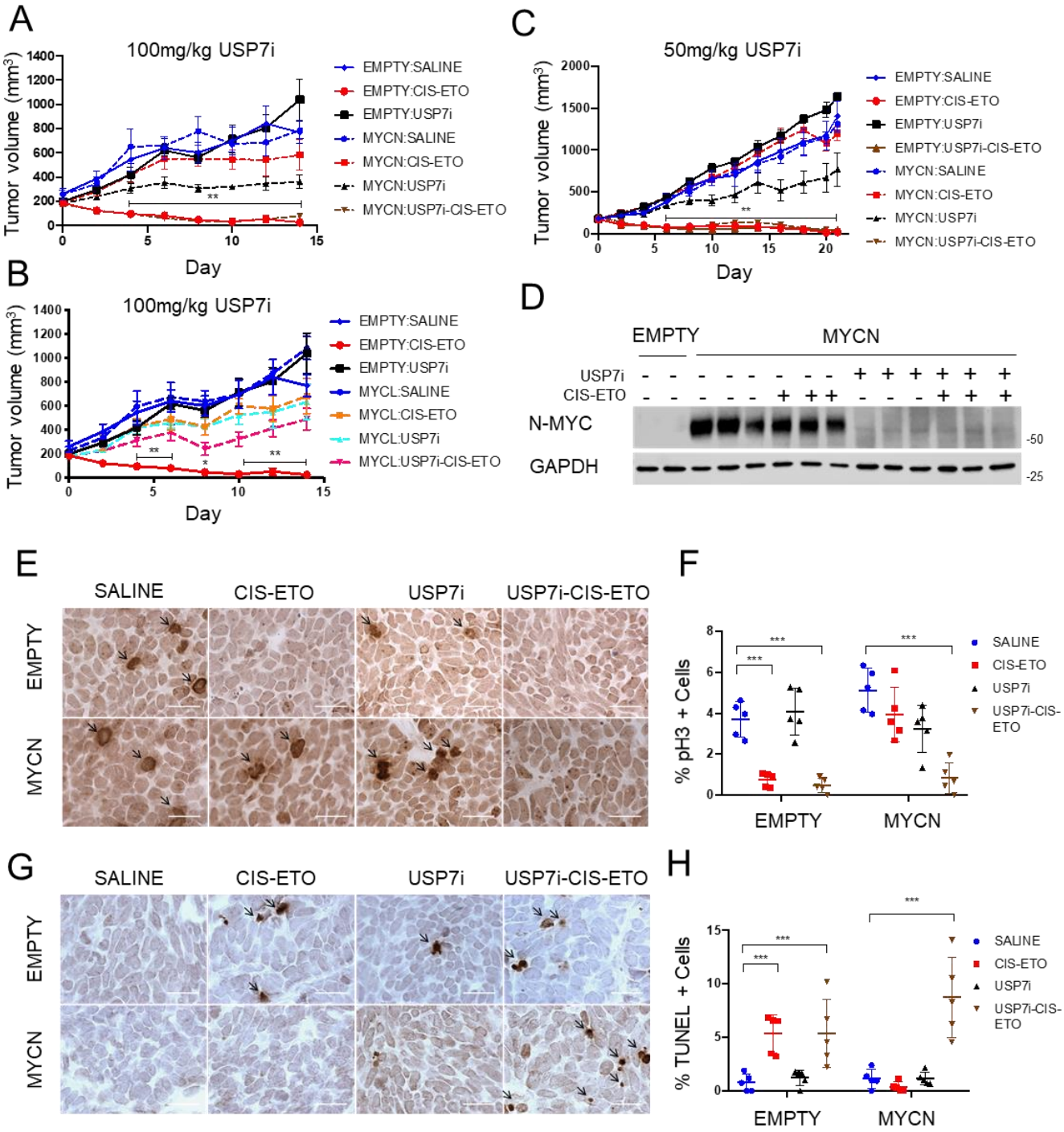


**Figure 2.7: USP7 inhibition re-sensitizes *MYCN*-overexpressing tumors to chemotherapy** (A) Graph showing flank tumor volumes of empty control vs. *MYCN* overexpressing FHSC14 PDX tumors over 14 days of treatment with either saline, cis-

eto, 100 mg/kg USP7i, or 100 mg/kg USP7i + cis-eto. Data are means ± SEM (n=5 in all groups except for EMPTY CIS-ETO and *MYCN* USP7i where n=4). Significance was determined using a mixed model two-way ANOVA followed by a posthoc Tukey's multiple comparisons test. For each group, significance is presented relative to the respective saline condition. **p<0.01 (B) Graph showing flank tumor volumes of empty control vs. *MYCL* overexpressing FHSC14 PDX tumors over 14 days of treatment with either saline, cis-eto, 100 mg/kg USP7i, or 100mg/kg USP7i + cis-eto. Data are means ± SEM (n=5 in all groups except for EMPTY CIS-ETO, *MYCL* SALINE, and *MYCL* USP7i + CIS/ETO where n=4. EMPTY samples are the same as in (A)). Significance was determined using a mixed model two-way ANOVA followed by a posthoc Tukey's multiple comparisons test. For each group, significance is presented relative to the respective saline condition. *p<0.05, **p<0.01 (C) Graph showing flank tumor volumes of empty control vs. *MYCN* overexpressing FHSC14 PDX tumors over 21 days of treatment with either saline, cis-eto, 50mg/kg USP7i, or 50mg/kg USP7i + 1 cycle of cis-eto. Data are means ± SEM (n=5 in all groups). Significance was determined using a mixed model two-way ANOVA followed by a posthoc Tukey's multiple comparisons test. For each group, significance is presented relative to the respective saline condition,**p<0.01. (D) Immunoblot comparing levels of N-MYC expression across treatment groups after 7 days of treatment in a parallel cohort. GAPDH was used as a loading control. (E) Representative immunohistochemistry images for pH3 staining comparing treatment groups. Scale bar = 20μm (F) Quantification of % pH3 positive cells. Data are means ± SEM (n=5 in all groups). Significance was determined using two-tailed unpaired Student's t test. ***p<0.001. (G) Representative immunohistochemistry images for TUNEL staining comparing treatment groups. Scale

bar = 20μm (H) Quantification of % TUNEL positive cells. Data are means ± SEM. (n=5 in all groups). Significance was determined using two-tailed unpaired Student's t test. ***p<0.001.

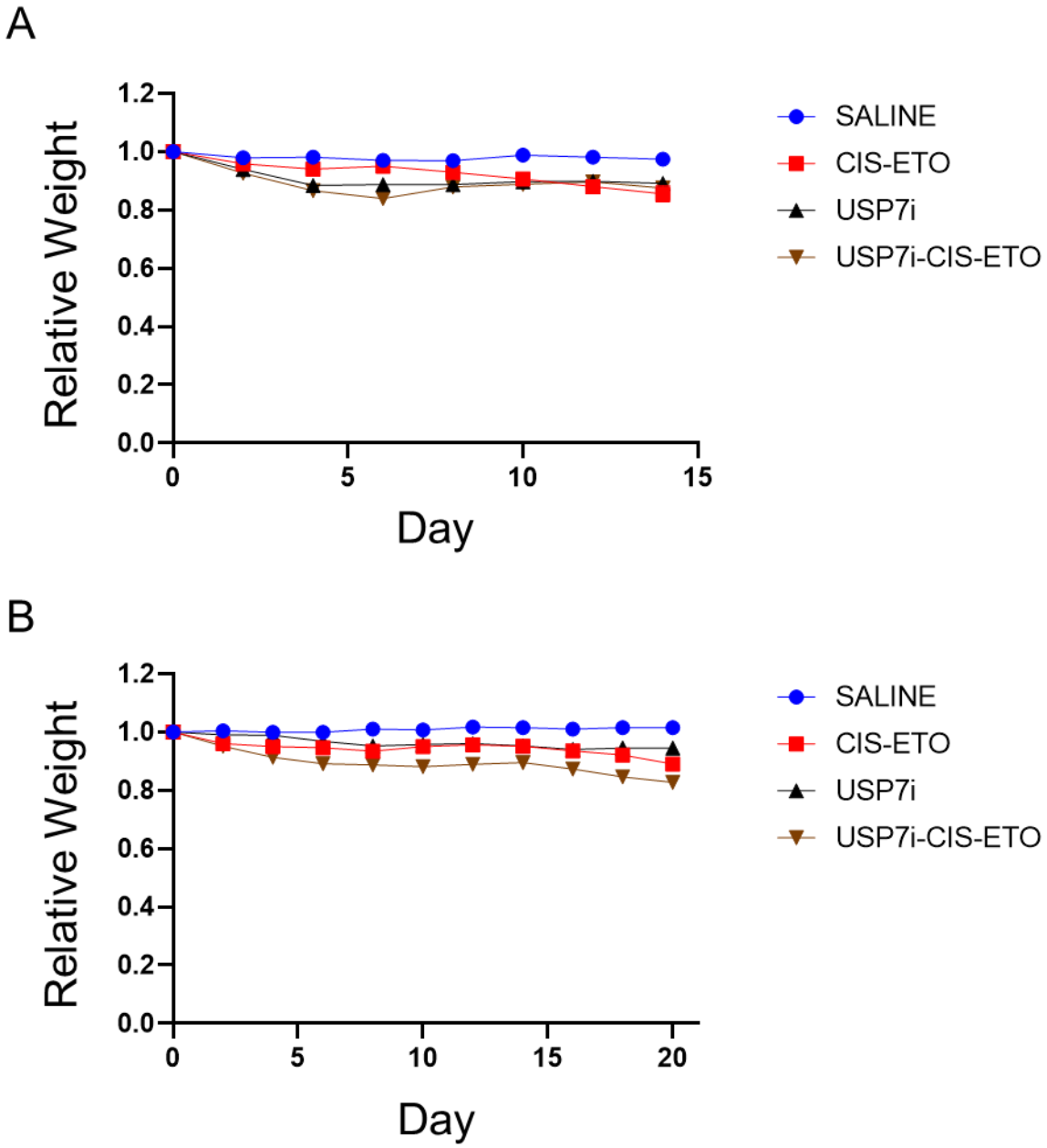

**Figure 2.8: Weight changes in response to treatment regimens** (A) Graph showing weight change relative to baseline of all mice in the treatment cohorts described in Fig. 2.7A, B. (B) Graph showing weight change relative to baseline of all mice in the treatment cohorts described in Fig. 2.7C.

# CHAPTER 3- Identifying Drivers of SCLC Chemoresistance Using in In Vivo Screens

## 3.1 Investigating SCLC Chemoresistance Using a Genome Wide CRISPR-Cas9 Screen

Having had success in validating *MYCN* and *MYCL* as drivers of SCLC chemoresistance, we sought to use our novel model systems to broadly investigate potential drivers of chemoresistance in SCLC. In the previous chapter, we demonstrated the ability to use lentiviral infection to generate stable PDX models that express constructs of interest. We applied that same approach to modify chemsensitive PDX models using a previously established CRISPR-Cas9 sgRNA library. In a pilot experiment, we extracted cells from FHSC14 tumors and then infected with lentivirus containing the Human GeCKO Lentiviral sgRNA Library v2 vector system, which expresses a pool of 123,411 sgRNAs targeting 19,050 genes (Sanjana 2014). Following infection, we collected a small portion of cells for an early timepoint (P0) and injected the remaining population into a cohort of NSG mice. Once flank tumors developed and reached 150mm$^3$, we divided the mice into saline and cis-eto treatment groups. Mice in the saline group were given weekly injections of saline until flank tumors reached a volume of 1000mm$^3$, at which point tumors were harvested and snap frozen. Mice in the

cis-eto group were given 3 weekly cycles of cis-eto treatment over the course of 21 days after which tumors were collected and snap frozen. We then extracted tumor DNA and pooled an equimolar amount of DNA from each tumor to generate Saline Pool and Cis-Eto Pool samples respectively. We performed deep sequencing and compared the abundance of sgRNAs in the Saline Pool and Cis-Eto Pool relative to the P0 population (Fig. 3.1). Using MAGeCK-VISPR analysis, we generated a ranked list of genes that were enriched in the Cis-Eto Pool relative to the P0 population (Table 3.1). However, the enrichment of only 3 of those genes was found to be statistically significant using FDR analysis, likely reflecting substantial heterogeneity between the individual tumors that made up each Pool. Analysis of individual sgRNAs showed that in both the Saline and Cis-Eto Pools, the vast majority of genes had between 0-3 corresponding sgRNAs enriched relative to the P0 condition (Fig. 3.2A, B). Notably, several genes that code for members of the SAGA pathway (*USP22, TADA1, TAF5L*) were found to have 4-5 corresponding sgRNAs enriched in the Cis-Eto Pool, a finding that was not observed in the Saline Pool (Fig. 3.2A, B, Table A.1, A.2). To date, the SAGA complex has yet to be extensively studied in SCLC and these results provide the first hint that this pathway may play a role in regulating SCLC chemoresistance.

Other studies utilizing in vivo screens in xenograft models have suggested a potential bottleneck effect in which there is an upper limit of sgRNAs that will ultimately be observed in a flank tumor regardless of the number of cells present in the initial injection (Chen 2015, Chow 2018). To assess if this was the case in our system as well, we performed deep sequencing on 4 of the individual tumors in the saline cohort to determine the number of unique sgRNAs present in each tumor. In doing so, we found

that we were only able to detect at most ~38,000 unique sgRNAs in an individual tumor. The average number of guides detected was 17,155 which represents only 14% of the total library (Table 3.2). As such, any analysis of our genome wide screen is limited by the fact that only a fraction of the library is present in any given tumor even before the start of cis-eto treatment, thereby complicating robust statistical due to a high rate of false negatives. In response to this analysis, we shifted our in vivo screening strategy to account for this bottlenecking effect.

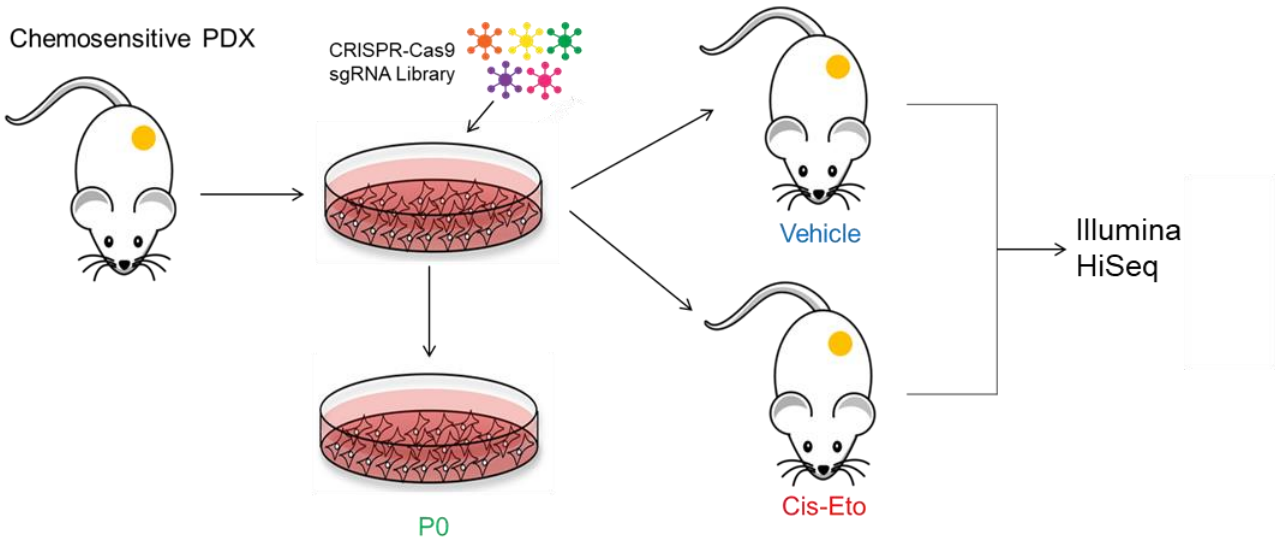


**Figure 3.1: Workflow of in vivo CRISPR-Cas9 screens.** Schematic outline of in vivo CRISPR-Cas9 screens from extraction through collection.

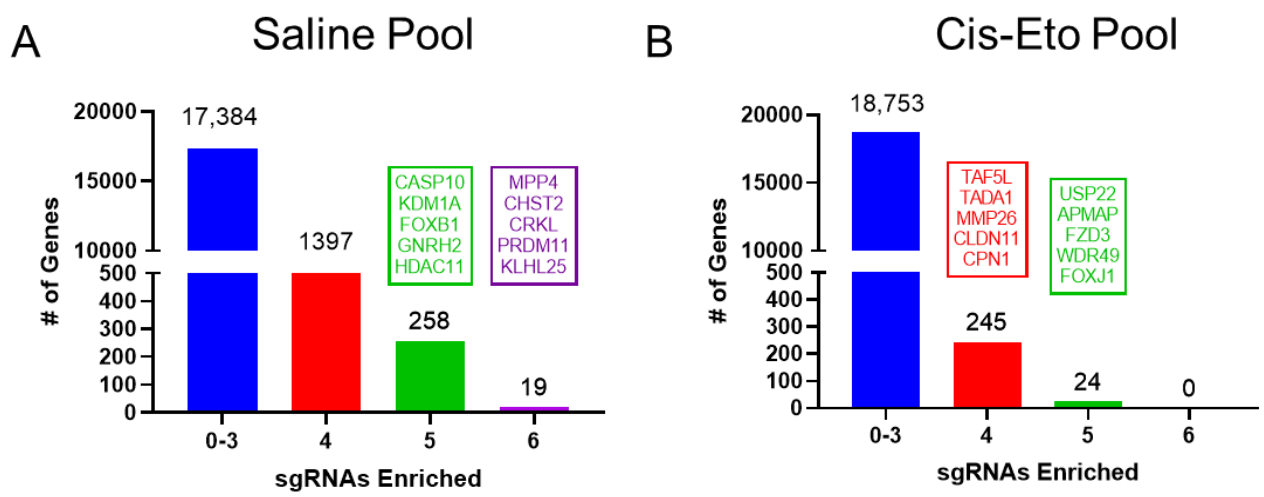


**Figure 3.2: Analysis of the Genome-wide FHSC14 Screen** (A) Number of genes with 0-3, 4, 5, or 6 significantly enriched sgRNAs targeting that gene in the Saline Pool. Panels above bars show genes exhibiting greatest log fold change relative to the P0. (B) Number of genes with 0-3, 4, 5, or 6 significantly enriched sgRNAs targeting that gene in the Cis-Eto Pool. Panels above bars show genes exhibiting greatest log fold change relative to the P0.

| Gene | FDR<0.1 | # sgRNAs Enriched |
|---|---|---|
| hsa-mir-6867 | yes | 3/4 |
| TAF5L | yes | 4/6 |
| USP22 | yes | 5/6 |
| AMPAP | no | 5/6 |
| PPP3CC | no | 3/6 |
| HFE2 | no | 4/6 |
| SUMO1 | no | 2/6 |
| FOXJ1 | no | 5/6 |
| TADA1 | no | 4/6 |
| ZNF485 | no | 5/6 |

**Table 3.1: Top ranked genes in the Cis-Eto-Pool.** Table showing 10 most enriched genes in the Cis-Eto Pool relative to the P0 as determined using MAGeCK-VISPR analysis of the genome-wide FHSC14 screen.

| Tumor | sgRNAs Detected | % of Library Detected |
|---|---|---|
| FHSC14_SAL_1 | 38,365/122,411 | 31.3 |
| FHSC14_SAL_2 | 8,517/122,411 | 7.0 |
| FHSC14_SAL_3 | 14,637/122,411 | 12.0 |
| FHSC14_SAL_4 | 7,101/122,411 | 5.8 |

**Table 3.2: Guides detected in individual tumors.** Table showing the number of sgRNAs detected following sequencing of three individual saline treated tumors from the genome-wide FHSC14 screen.

### 3.2 Investigating SCLC Chemoresistance Using a Focused CRISPR-Cas9 Screen

Due to limitations in the number of cells that can go on to seed a flank tumor, we designed a custom, small, focused sgRNA library with an emphasis on genes potentially relevant in SCLC. This library (herein referred to as Focused SCLC library) contains sgRNAs targeting 400 genes with 6 sgRNAs per gene along with 120 non-targeting sgRNAs. The genes for this library were chosen based on various sources including: genes frequently mutated in human SCLC, genes that had 4 or 5 sgRNAs enriched in the genome wide screen described above, and genes that were found to be enriched in cis-eto treated *MYCN*- or *MYCL*-overexpressing tumors (Fig. 3.3, Table A.3). Once

designed, the Focused SCLC library was assembled into a lentiviral vector system as part of a collaboration with the Paddison Lab.

We extracted cells from FHSC14 tumors and infected with lentivirus containing the Focused SCLC library system. Following infection, we harvested a small portion of cells to use as a P0 population and then injected the remaining cells into a cohort of NSG mice (Focused SCLC FHSC14-1) (Table 3.3). Once flank tumors developed and reached a volume of 150mm$^3$, we divided the mice into saline and cis-eto treatment groups as outlined in Fig. 3.1. Mice in the saline group were given weekly saline treatment until tumors reached a volume of 1000mm$^3$, at which point tumors were collected and snap frozen. Mice in the cis-eto treatment group were given six cycles of cis-eto treatment over the course of 10 weeks after which tumors were collected and snap frozen. Once all tumors were collected, we extracted DNA and performed deep sequencing to determine the abundance of sgRNAs present in each saline and cis-eto treated tumor as well as the P0 population. Analysis of the distribution of sgRNAs in each saline treated tumor revealed that only a small number of sgRNAs targeting a given gene were prevalent at greater than 1.5% of all reads in any given tumor (Fig. 3.4A). In the cis-eto treated tumors, even fewer sgRNAs were prevalent at greater than 1.5% of all reads in any given tumor. Notably, sgRNAs targeting *SLFN11*, the only previously reported gene whose inactivation has been linked to SCLC chemoresistance (Gardner 2017), were present at greater than 10% of total reads in one of the tumors, potentially indicating a chemoresistant colony (Fig. 3.4B). Furthermore, sgRNAs targeting *USP22*, one of the highest ranked genes in the Cis-Eto Pool of the genome-wide screen, were prevalent at greater than 1.5% of total reads in multiple cis-eto

tumors (Fig. 3.4B). Next, we used MAGeCK analysis to identify sgRNAs that were enriched in either the saline or cis-eto treated tumors relative to the P0 population. In the saline treated tumors, we observed that while the vast majority of genes had 0 or 1 corresponding sgRNAs enriched relative to the P0 condition, 43 genes had multiple sgRNAs enriched (Fig. 3.4C, Table A.4). These genes included *PTEN*, a well-known tumor suppressor, and *BAX*, a key effector of apoptosis. As such, enrichment of multiple sgRNAs in the saline tumors is likely indicative of genes whose loss confers a pro-proliferative effect on SCLC. Similarly, analysis of the cis-eto treated tumors revealed that only 22 genes had more than 2 corresponding sgRNAs enriched relative to the P0 population (Fig. 3.4D, Table A.5). These genes included *SLFN11* and *USP22*, further indicating that loss of these genes may confer chemoresistance in SCLC. Additionally, we used MAGeCK-MLE analysis to generate a ranked list of genes whose loss was enriched in the cis-eto treated tumors at a greater extent than in the saline treated tumors. Once again, genes such as *SLFN11* and *USP22* are found at the top of this list (Fig. 3.4E, F). Taken together, the analysis of our Focused SCLC screen identified several potential candidates, such as *USP22*, for subsequent validation as possible drivers of chemoresistance in SCLC.

To determine if our observations were consistent across multiple experiments, we set up another in vivo screen using the Focused SCLC library. As in the above experiment, we extracted cells from FHSC14 tumors, infected with lentivirus containing the Focused SCLC library system, and injected cells into a new cohort of NSG mice after harvesting a small portion to use as a P0 condition (Focused SCLC FHSC14-2) (Table 3.3). As in the first experiment, mice in the saline group were given weekly saline treatment until

tumors were collected upon reaching 1000mm$^3$ while mice in the cis-eto group were treated with 6 cycles of cis-eto chemotherapy over the course of 10 weeks at which point tumors were collected. Following tumor collection, we used deep sequencing to determine the abundance of sgRNAs in each condition. Analysis of the distribution of sgRNAs in the saline treated tumors again showed that relatively few sgRNAs targeting a given gene were prevalent at greater than 1.5% of total reads in any given tumor with no one gene predominant (Fig. 3.5A). However, in the cis-eto condition, while most tumors did not exhibit sets of sgRNAs found at high abundance, there was one tumor in which sgRNAs targeting either *TAF5L* or *NSD1* accounted for 30% and 23% of all reads in the tumor respectively. Furthermore, sgRNAs targeting members of the SAGA complex (including *TAF5L, USP22*, and *TADA1*) were prevalent at greater than 1.5% in multiple tumors (Fig. 3.5B). Both of these observations are consistent with the development of clonal populations within tumors that are resistant to cis-eto treatment. We next used MAGeCK analysis to identify sgRNAs that were enriched in the saline or cis-eto treated tumors relative to the P0 timepoint. In the saline treated tumors, the majority of genes had only 0 or 1 corresponding sgRNAs enriched (Fig. 3.5C). Notably, we observed multiple genes that had 3 or 4 corresponding sgRNAs enriched, including genes whose loss is known to drive SCLC such as NOTCH family members (Fig. 3.5C, Table A.6) (Augert 2019). In the cis-eto treated tumors, we found that 382/400 genes had no corresponding sgRNAs enriched in the tumors relative to the P0. Of the 18 remaining genes, only 4 had multiple enriched corresponding sgRNAs (Fig. 3.5D, Table A.7). Remarkably, all 4 of these genes (*USP22, TAF5L, TADA1, TADA2B*) were members of the SAGA complex, strongly suggesting that this pathway could play an

important role in mediating SCLC chemoresistance. Using MAGeCK-MLE, we generated a ranked list of genes ordered by greatest enrichment in the cis-eto treated tumors relative to enrichment in the saline treated tumors. In doing so, we found that 5 of the top 10 genes in this list (*USP22, TAF5L, TAF6L*, *TADA1, TADA2B*) were members of the SAGA complex (Fig. 3.5E, F). Taken in concert, our findings from both cohorts of the FHSC14 Focused SCLC screen identify the SAGA complex, particularly *USP22*, as a novel high priority target for subsequent validation as a potential driver of chemoresistance in SCLC.

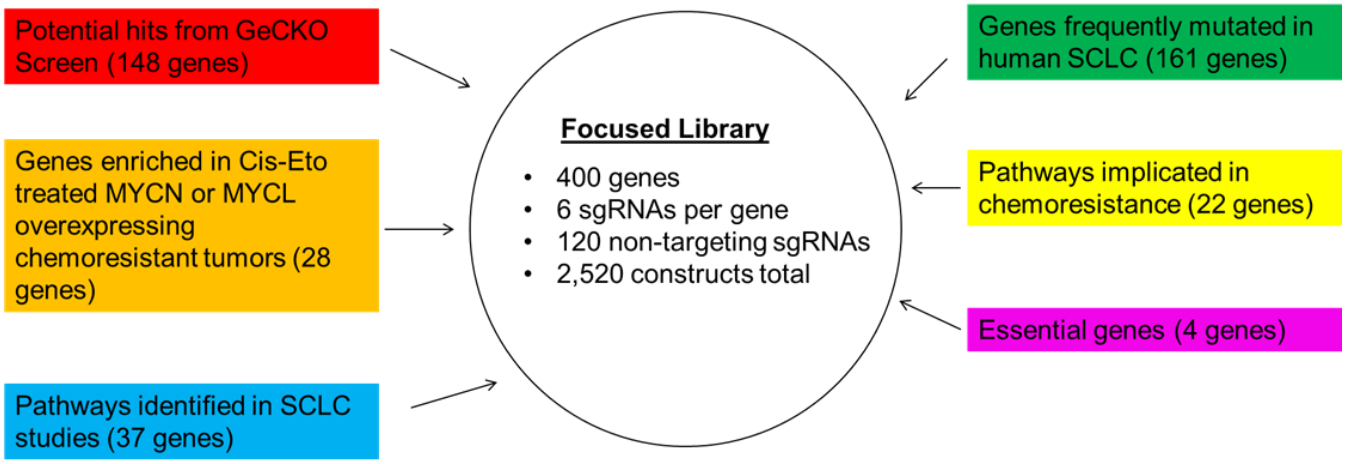


**Figure 3.3: Design of Focused SCLC library.** Summary of sources used to design the Focused SCLC library. Colored panels show rationales for gene selection.

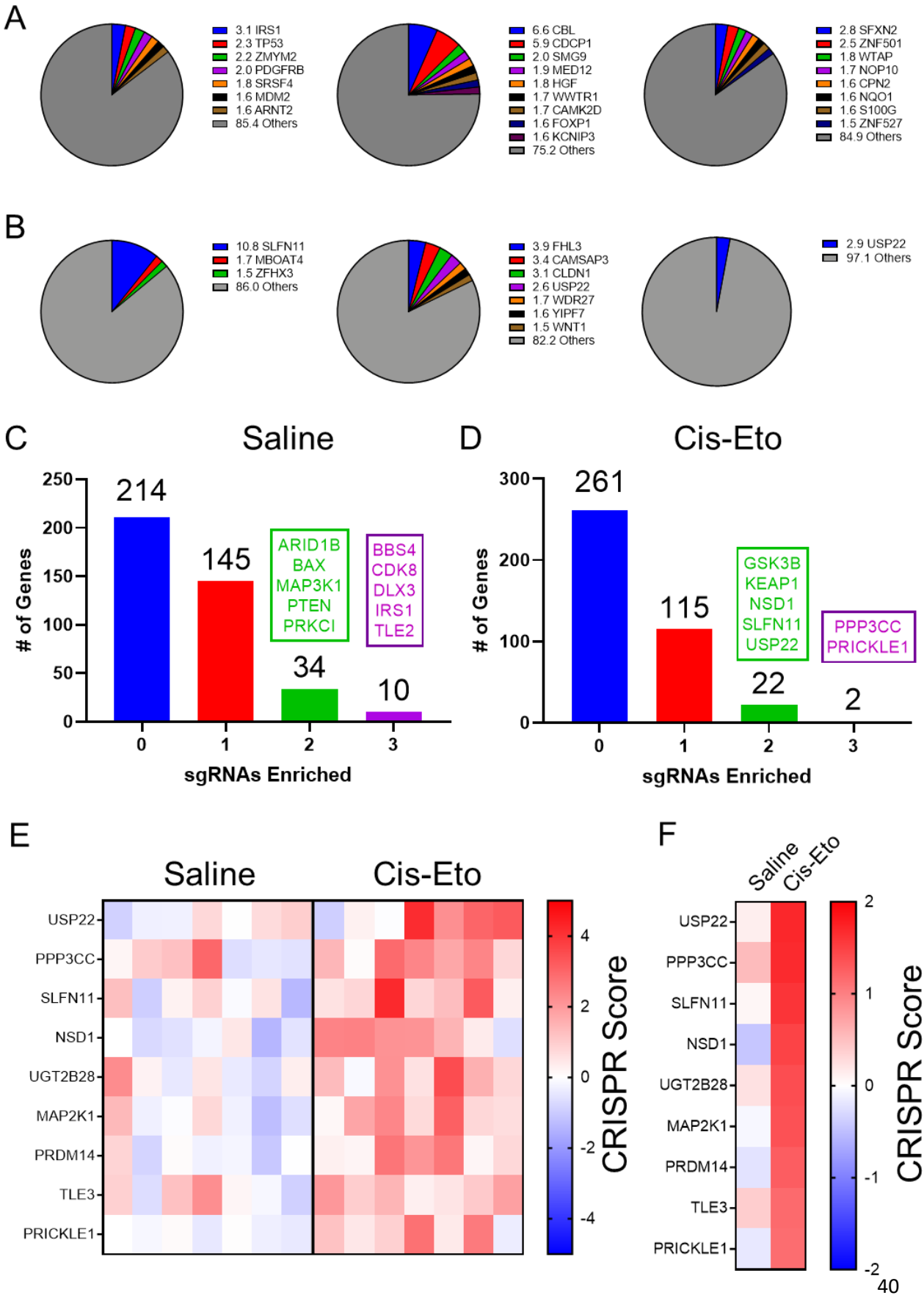
A
3.1 IRS1
2.3 TP53
2.2 ZMYM2
2.0 PDGFRB
1.8 SRSF4
1.6 MDM2
1.6 ARNT2
85.4 Others
6.6 CBL
5.9 CDCP1
2.0 SMG9
1.9 MED12
1.8 HGF
1.7 WWTR1
1.7 CAMK2D
1.6 FOXP1
1.6 KCNIP3
75.2 Others
2.8 SFXN2
2.5 ZNF501
1.8 WTAP
1.7 NOP10
1.6 CPN2
1.6 NQO1
1.6 S100G
1.5 ZNF527
84.9 Others
B
10.8 SLFN11
1.7 MBOAT4
1.5 ZFHX3
86.0 Others
3.9 FHL3
3.4 CAMSAP3
3.1 CLDN1
2.6 USP22
1.7 WDR27
1.6 YIPF7
1.5 WNT1
82.2 Others
2.9 USP22
97.1 Others
C
Saline
# of Genes
214
145
34
10
ARID1B
BAX
MAP3K1
PTEN
PRKCI
BBS4
CDK8
DLX3
IRS1
TLE2
sgRNAs Enriched
D
Cis-Eto
# of Genes
261
115
22
2
GSK3B
KEAP1
NSD1
SLFN11
USP22
PPP3CC
PRICKLE1
sgRNAs Enriched
E
Saline
Cis-Eto
USP22
PPP3CC
SLFN11
NSD1
UGT2B28
MAP2K1
PRDM14
TLE3
PRICKLE1
CRISPR Score
F
Saline
Cis-Eto
USP22
PPP3CC
SLFN11
NSD1
UGT2B28
MAP2K1
PRDM14
TLE3
PRICKLE1
CRISPR Score

**Figure 3.4: Analysis of the Focused SCLC FHSC14-1 screen.** Pie charts showing the most prevalent genes in the tumors of three representative saline (A) and cis-eto (B) treated mice. (C) Number of genes with 0, 1, 2, or 3 significantly enriched sgRNAs targeting that gene in the saline treated tumors. Panels above bars show selected genes. (D) Number of genes with 0, 1, 2, or 3 significantly enriched sgRNAs targeting that gene in the cis-eto treated tumors. Panels above bars show selected genes. (E) Heatmap showing CRISPR scores of selected genes for each saline and cis-eto treated tumor. Genes were selected based on statistical significance from MAGECK-MLE analyses and ordered by greatest difference in saline and cis-eto β-scores. (F) Heatmap showing average CRISPR scores of selected genes in the saline and cis-eto treated cohorts.

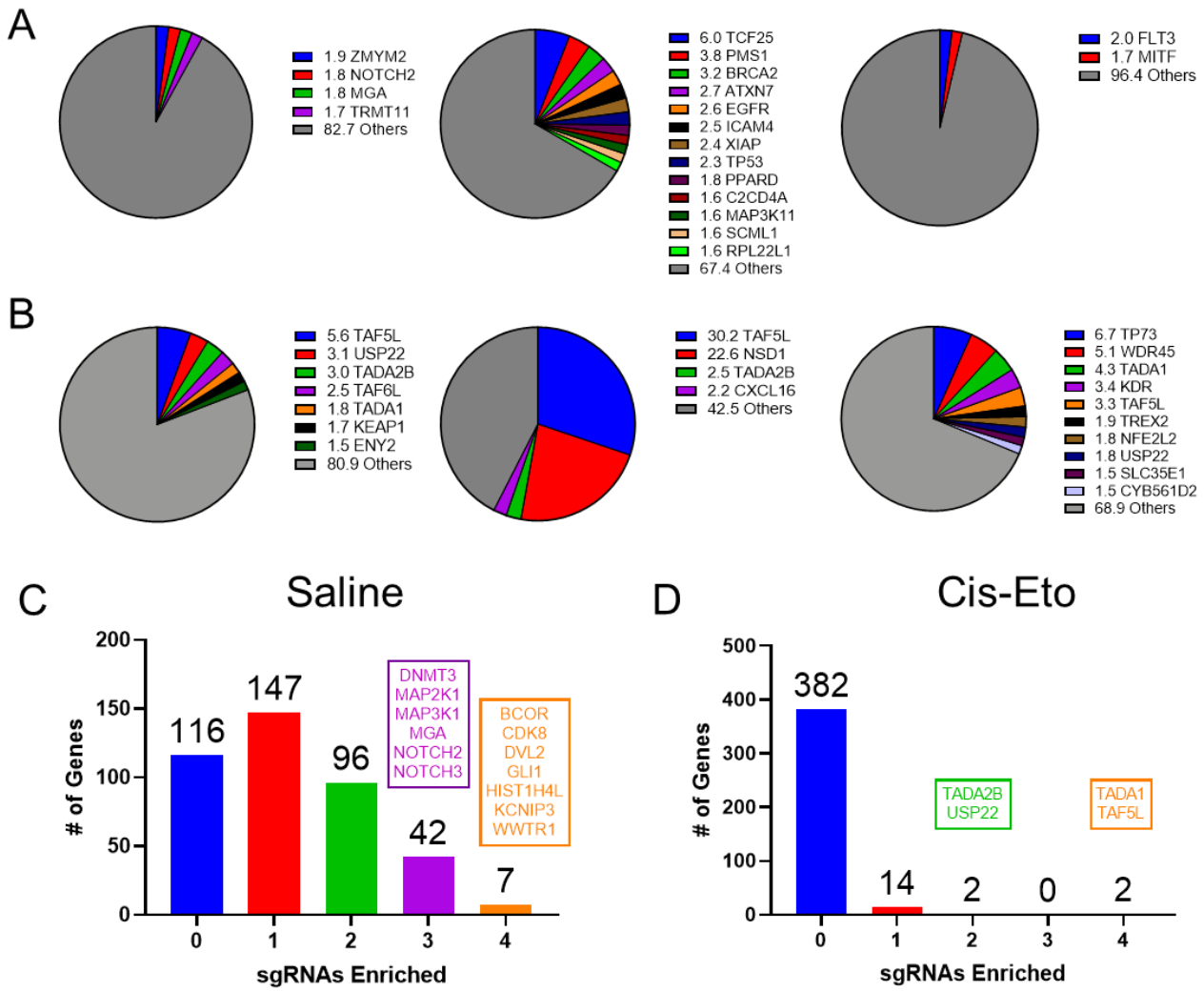
A
1.9 ZMYM2
1.8 NOTCH2
1.8 MGA
1.7 TRMT11
82.7 Others
6.0 TCF25
3.8 PMS1
3.2 BRCA2
2.7 ATXN7
2.6 EGFR
2.5 ICAM4
2.4 XIAP
2.3 TP53
1.8 PPARD
1.6 C2CD4A
1.6 MAP3K11
1.6 SCML1
1.6 RPL22L1
67.4 Others
2.0 FLT3
1.7 MITF
96.4 Others
B
5.6 TAF5L
3.1 USP22
3.0 TADA2B
2.5 TAF6L
1.8 TADA1
1.7 KEAP1
1.5 ENY2
80.9 Others
30.2 TAF5L
22.6 NSD1
2.5 TADA2B
2.2 CXCL16
42.5 Others
6.7 TP73
5.1 WDR45
4.3 TADA1
3.4 KDR
3.3 TAF5L
1.9 TREX2
1.8 NFE2L2
1.8 USP22
1.5 SLC35E1
1.5 CYB561D2
68.9 Others
C
Saline
# of Genes
200
150
100
50
0
116
147
96
42
7
DNMT3
MAP2K1
MAP3K1
MGA
NOTCH2
NOTCH3
BCOR
CDK8
DVL2
GLI1
HIST1H4L
KCNIP3
WWTR1
0
1
2
3
4
sgRNAs Enriched
D
Cis-Eto
# of Genes
500
400
300
200
100
0
382
14
2
0
2
TADA2B
USP22
TADA1
TAF5L
0
1
2
3
4
sgRNAs Enriched
E
Saline
Cis-Eto
TAF5L
TADA1
USP22
TADA2B
TP73
TAF6L
NSD1
FAS
SCML1
KEAP1
5
0
-5
CRISPR Score
F
Saline
Cis-Eto
TAF5L
TADA1
USP22
TADA2B
TP73
TAF6L
NSD1
FAS
SCML1
KEAP1
4
2
0
-2
-4
CRISPR Score

**Figure 3.5: Analysis of the Focused SCLC FHSC14-2 Screen.** Pie charts showing the most prevalent genes in the tumors of three representative saline (A) and cis-eto (B) treated mice. (C) Number of genes with 0, 1, 2, 3, or 4 significantly enriched sgRNAs targeting that gene in the saline treated tumors. Panels above bars show selected genes. (D) Number of genes with 0, 1, 2, 3, or 4 significantly enriched sgRNAs targeting that gene in the cis-eto treated tumors. Panels above bars show selected genes. (E) Heatmap showing CRISPR scores of selected genes for each saline and cis-eto treated tumor. Genes were selected based on statistical significance from MAGECK-MLE analyses and ordered by greatest difference in saline and cis-eto β-scores. (F) Heatmap showing average CRISPR scores of selected genes in the saline and cis-eto treated cohorts.

| Cohort | Total Mice | # of Saline Treated Tumors | # of Cis-Eto Treated Tumors |
|---|---|---|---|
| Genome-wide FHS14 | 12 | 11 | 12 |
| Focused SCLC FHSC14-1 | 14 | 7 | 7 |
| Focused SCLC FHSC14-2 | 10 | 5 | 5 |

**Table 3.3: In vivo CRISPR-Cas9 screen cohorts.** Table showing number of mice used in each in vivo CRISPR-Cas9 screen cohort along with number of tumors collected for

each condition. For the Genome-wide FHSC14 cohort, tumor cells were injected into both flanks of each mouse.

## CHAPTER 4- Materials and Methods

**Genetically Engineered Mouse Models.** *Rb1*$^{lox/lox}$ mice were from Tyler Jacks (MIT) while *Trp53*$^{lox/lox}$ mice were generated by Dr. Anton Berns (Netherlands Cancer Institute) (Meuwissen 2003). The generation of the *RPMYCL* model has been previously described and the generation of the *RPMYCN* model by our lab is described elsewhere (Huijbers 2014). Tumor formation was initiated by intratracheal infection of adult mice with either Ad-CMV-Cre (*RP* and *RPMYCL*) or Ad-CGRP-Cre (*RPMYCN*) at a titer of 1.25 x $10^9$ pfu/mouse (DuPage 2009). Both Ad-CMV-Cre and Ad-CGRP-Cre were obtained from the University of Iowa Gene Vector Core. To induce transgene activation, all *RPMYCN* mice were given feed containing doxycycline (DOX feed, Teklad) beginning at one week following intratracheal infection and continuing throughout the course of the study. Lung tumor burden was assessed using magnetic resonance imaging. In all studies involving GEM models, lung tumor fragments were collected for both molecular analyses (snap frozen) and immunohistochemistry (fixed in neutral buffered formalin). All animal procedures were approved by the Institutional Animal Care and Use Committee (IACUC) at the Fred Hutchinson Cancer Research Center.

**Western Blot Analysis.** Protein was extracted from lung tumor and PDX tumor tissues by dissociation in RIPA buffer (Cell Signaling, 9806). Dissociation was performed by mechanical disruption. Immunoblotting by western blot was performed according to standard procedures. The following antibodies were used: anti-N-MYC (Cell Signaling,

51705, 1:500), anti-β ACTIN (Cell Signaling, 4970, 1:2000), anti-LMYC (in house, 1:8000), anti-cleaved CASPASE3 (Cell Signaling, 9661, 1:500), anti-GAPDH (Santa Cruz, sc-32233, 1:1000).

**Histology and Immunohistochemistry.** Mouse lung tumor and PDX tumor fragments were fixed in neutral-buffered formalin for 48 hours prior to processing to paraffin blocks. Paraffin blocks were sectioned at a thickness of 4µm. For immunohistochemistry analysis, paraffin sections were dewaxed in xylene and then rehydrated by passage through a graded series of ethanol into Tris buffered saline-Tween 20 (TBS-T). Antigen unmasking was performed by heating in a tiered steamer in Trilogy buffer (Cell Marque, 920-P) according to the manufacturer's protocol. Endogenous peroxidases were blocked with 3.5% $H_2O_2$ and sections were incubated overnight at 4°C in primary antibody following blocking with 5% goat serum (Jackson ImmunoResearch, 005-000-121). The following primary antibodies were used: anti-phospho Ser10 histone H3 (EMD Millipore, 06-570, 1:100). Sections were then incubated with biotin-conjugated secondary antibodies (Vector Laboratories, BA-1000, 1:100) after which a biotin-peroxide complex was formed using the Vectastain ABC kit (Vector Laboratories, PK-4000) Detection was carried out using 3,3'-diaminobenzidine substrate (Vector Laboratories, SK-4100). TUNEL assays were performed using the POD in situ cell death detection kit (Roche, 11684817910) according to the manufacturer's protocol. Slides were imaged using a Nikon E800 microscope and quantified at 100x magnification with three fields per section.

**PDX Model Generation.** The generation and characterization of the FHSC14 PDX model has been described previously (Augert 2019). The FHSC23 PDX model was

generated from the circulating tumor cells of a chemonaive SCLC patient using previously described methodology (Hodgkinson 2014). Both models are propagated in the flanks of NOD-SCID-gamma (NSG) mice. To generate *MYCN*- and *MYCL*-overexpressing PDX models described in Figures 2.2 and 2.3, human *MYCN* or *MYCL* cDNA was cloned into the pLX304 lentiviral vector backbone (Addgene, 25890) using Gibson assembly to generate pLX304 *MYCN* and pLX304 *MYCL* plasmids (Yang 2011). A pLX304 plasmid containing a stuffer sequence (pLX304 EMPTY) was used as a control vector. Lentivirus was generated by co-transfection of 293TN cells with either pLX304 EMPTY, *MYCN*, or *MYCL* plasmid along with packaging plasmids psPAX2 (Addgene, 12260) and pMD2.G (Addgene, 12259) using a calcium phosphate transfection protocol (Beronja 2010). Viral supernatants were collected 64 hours post-transfection, filtered through a 0.45µM filter, and concentrated using a Centricon-70 system (EMD Millipore, UFC710008). Virus was resuspended in sterile PBS. For infection, PDX tumors were resected and digested for 20 minutes at 37°C in 1mg/mL collagenase (Sigma, C5138) in PBS. Digested tissue was sequentially strained through a 70µM and 40µM mesh to generate a single cell suspension which was then plated in DMEM-F12 media. Cells were then incubated with virus for a total of 16 hours after which they were collected, spun down, mixed 1:1 with Matrigel (Corning, CB-40234) and re-injected into NSG mice. To generate the *MYCN* and *MYCL* overexpressing PDX models described in Figure 2.7, human *MYCN* or *MYCL* cDNA was cloned into a pLVX-IRES-ZsGreen lentiviral vector backbone using Gibson assembly to generate pLVX *MYCN*, pLVX *MYCL*, or pLVX empty vectors (Pelish 2015). Virus production and infection of FHSC14 cells was carried out as described above with the exception that

cells were injected after 4 hours of incubation with virus. Once tumors from infected FHSC14 cells grew out, the tumors were collected, digested as described above and sorted using the FITC channel of an Aria 2 cell sorter. Sorted cells were re-injected into NSG mice and allowed to grow out. Tumors from these mice were then collected, digested and put through another round of sorting to generate pure populations of FHSC14 *MYCN*, FHSC14 *MYCL*, and FHSC14 empty control cells (Fig. 2.6) that were then re-injected into NSG mice. To generate the sgRNA library expressing PDX models described in Chapter 3, we extracted cells from FHSC14 tumors and infected with lentivirus containing the Human GeCKO Lentiviral sgRNA Library v2 pool or our Focused SCLC library (Sanjana 2014). Following infection and separation of P0 timepoints, cells were re-injected into NSG mice either at 16 hours (Genome-wide FHSC14 screen and Focused SCLC FHSC14-1 screen) or 4 hours (Focused SCLC FHSC14-2 screen) post infection as described above.

**Drug Treatment Studies.** For the experiments described in Figure 2.1, *RP*, *RPMYCL*, and *RPMYCN* mice with sufficient tumor burden (as determined by MRI imaging) were randomly assigned to saline or cis-eto treatment groups. Mice in the saline group were treated weekly with saline while mice in the cis-eto group were treated with 3 weekly cycles of chemotherapy consisting of 5mg/kg cisplatin (Sigma, 479306) on day 1 and 10mg/kg etoposide (Sigma, E1383) on days 1,2, and 3. Thoracic MR images were collected on days 0, 14, and 21 and tumor volume was calculated using ImageJ.

For the experiments described in Figures 2.2, 2.3, and 2.7 NSG mice were implanted with $1.0x10^6$ disaggregated cells from the modified FHSC14 or FHSC23 PDX models as described above. Flank tumors were measured using calipers and tumor volume was

calculated using the formula for a prolate ellipsoid: $V=D*(d^2/2)$, where V is volume, D is the major axis of the tumor and d is the minor axis of the tumor (Hodgkinson 2014). Once flank tumor volume reached 150-250$mm^3$, mice were randomized into saline, cis-eto, USP7i, or USP7i-cis-eto treatment groups. Mice in the saline and cis-eto groups were treated as described above. Mice in the USP7i group were treated with a daily dose of either 100mg/kg (Fig 2.7A, B) or 50mg/kg (Fig. 2.7C) from days 0-7 and days 15-21. Mice in the USP7i-cis-eto treatment group were given both USP7i and cis-eto treatments as described above. In this group, both USP7i and cis-eto treatment regimens were not given for days 8-14.

For the experiments described in Chapter 3.1, mice were given saline or cis-eto treatment as described above. For the experiments described in Chapter 3.2, mice were given saline treatment as described above or cis-eto treatment consisting of 6 cycles of 5mg/kg cisplatin (day 1) and 10mg/kg etoposide (days 1-3) over the course of 10 weeks. Mice in these cohorts were given 2 week long drug holidays after exhibiting weight loss greater than 10% of initial body weight (on average after 2 or 3 cycles of chemotherapy). Once treatment resumed following a drug holiday, mice were given an additional drug holiday if they exhibited weight loss greater than 5% of body weight at the time when treatment resumed. All mice completed 6 cycles of chemotherapy by the conclusion of 10 weeks. All protocols were approved by the Fred Hutchinson Cancer Research Center IACUC.

**Genome Wide CRISPR-Cas9 Screen (Cell Lines).** Cells from 3 *RP* and 3 *RPMYCN* cell lines were cultured in DMEM complete media containing 1μM doxycycline. ~$400x10^6$ cells from each line were infected at MOI<1 with lentivirus containing the

Mouse GeCKO Lentiviral sgRNA Library v2 pool (Sanjana 2014). Cells were then placed under puromycin selection for 72 hours after which $65x10^6$ cells from each line were collected as a P0 reference while the remaining cells were passaged for 12 population doublings to generate a P12 end point. DNA was extracted using a previously described salt precipitation protocol (Chen 2015). sgRNA libraries were generated using a previously described PCR protocol and purified by running out on an agarose gel electrophoresis. The libraries were then quantified using a Kapa biosystems Library Quantification Kit (ThermoFisher, KK4824) and sequenced using an Illumina HiSeq 2500. Demultiplexed reads were trimmed and aligned to the Mouse GeCKO sgRNA Library using Bowtie (Langmead 2009). Using the sgRNA read counts, we generated CRISPR scores (as in (Wang 2015)). Non-targeting control guides were randomly binned in sets of 6 to generate a set of 166 NTC sgRNAs, prior to performing MAGeCK- MLE analysis to identify essential genes in *RP* and *RPMYCN* lines (Li 2014).

**Focused SCLC Library.** A full list of genes represented in the Focused SCLC library can be found in Table A.3. For each gene, 6 targeting sgRNAs were designed using the Graphical User Interface for DNA Editing Screens (GUIDES) tool (Meier 2017). 120 non-targeting sgRNAs were also designed to be used as negative controls. For each sgRNA, we designed oligonucleotides containing an sgRNA sequence, an upstream U6 promoter sequence, a scaffold sequence, and homology arms corresponding to the lentiCRISPR v2 vector (Sanjana 2014). Following the design phase, the final library consisting of 2,520 constructs was synthesized as a ssDNA oligo pool (Twist Biosciences). The oligo pool was then cloned into the lentiviral lentiCRISPR v2 vector using a previously described protocol (Sanjana 2014). We then generated high-titer

lentivirus containing the Focused SCLC library system using the calcium phosphate transfection and virus collection protocols described earlier in this chapter (Beronja 2010). The process of designing the individual sgRNAs through the cloning of the Focused SCLC library into the lentiCRISPR v2 vector system was done in collaboration with the Paddison Lab.

**In Vivo CRISPR-Cas9 Screen Analyses.** Following tumor collection in the experiments described in Chapter 3, samples were processed and sequenced as described in the section entitled, “Genome Wide CRISPR-Cas9 Screen (Cell Lines)”, earlier in this Chapter. Demultiplexed reads were aligned to either the Human GeCKO sgRNA Library or the Focused SCLC library respectively. Using the sgRNA read counts, we assessed the prevalence of a given gene in a tumor according to the formula: gene X prevalence = (Σ reads of all sgRNAs targeting gene X/ total reads in tumor)*100%. CRISPR scores were generated according the previously described formula. We used MAGeCK-VISPR analysis to assess enrichment of sgRNA in the saline or cis-eto treated tumors relative to the P0 condition (Li 2015). We considered an sgRNA to be enriched if it exhibited a log fold change > 1 relative to the P0 along with an FDR < 0.1. We used MAGeCK-MLE analysis to generate β-score values representing relative enrichment of each gene in either the saline or cis-eto conditions (Li 2014). Using these β-scores, we created a ranked gene list ordered according to Δ β-score ( Δ β-score = β-score (cis-eto) - β-score (saline)) as a measure of genes that were most enriched in the cis-eto treated tumors relative to the saline treated tumors.

**Statistics.** All plots and associated statistics were generated using GraphPad Prism 8. For Kaplan-Meier curves, significance was determined using a log-rank (Mantel-Cox)

test. For immunohistochemistry, immunofluorescence, cell cycle, cell proliferation, FACS, and MRI analyses significance between groups was determined using a two-tailed unpaired Student's t test. Mixed model two-way ANOVA was used to compare groups in the PDX model drug treatment studies. Significance was then determined using Tukey's multiple comparisons test. Statistics for analysis of the CRISPR-Cas9 screens were generated as part of the MAGeCK analysis algorithm (Li 2014).

## CHAPTER 5- Discussion

### 5.1 *MYCN* and *MYCL* Drive SCLC Chemoresistance

Using both GEM as well as isogenic PDX models of SCLC, we conclusively demonstrated that overexpression of either *MYCN* or *MYCL* was sufficient to confer chemoresistance. These results provide the first known evidence that *MYCN* can contribute to the development of SCLC chemoresistance in a robust in vivo model system. While previous studies utilizing *MYC*- and *MYCL*-overexpressing mouse models have included chemotherapy treatments, said studies did not use *RP* mice as a control arm (Mollaoglu 2017, Bottger 2019). As such, overall assessment of the contribution of either *MYC* or *MYCL* to chemotherapy response was impaired. Furthermore, a major limitation of studies utilizing GEM models of SCLC lies in the fact that tumor regressions in response to chemotherapy are rarely observed in this model system. As such, the absence of highly chemosensitive models of SCLC that regress upon cis-eto treatment has hindered the study of genetic drivers of SCLC chemoresistance. Our observation that two highly chemosensitive PDX models completely switch to becoming chemoresistant with *MYCN* or *MYCL* overexpression definitively show that these oncogenes can indeed drive chemoresistance in SCLC.

While further studies are needed to determine the molecular mechanisms through which MYC family members drive chemoresistance, our study highlights the critical roles that *MYCN* and *MYCL* play in the biology of SCLC and response to therapy.

We performed a comprehensive genome wide CRISPR-Cas9 screen on both *RP* and *RPMYCN* derived cell lines to uncover druggable vulnerabilities for *MYCN*-overexpressing SCLC. Our results revealed that multiple druggable targets such as *WEE1, BRD2*, and *USP7* are synthetically lethal with MYCN overexpression. *WEE1* has been extensively studied as a potential therapeutic target in SCLC (Sen 2017, Lallo 2018). Likewise, bromodomain and extra-terminal (BET) domain inhibitors that target proteins including *BRD2* and *BRD4* have shown efficacy in targeting *MYCL*- and *MYCN*-overexpressing SCLC cell lines (Leinhart 2015, Kato 2016). While the use of other USP7 inhibitors to target MYCN driven tumors has been studied in neuroblastoma (Tavana 2016), this approach has never been assessed in in vivo models of SCLC or in the context of chemoresistance. By using a novel inhibitor of USP7, we demonstrated that *MYCN*-overexpressing SCLC is highly sensitive to loss of USP7. Furthermore, using our PDX model system, we showed that pharmacological inhibition of USP7 can completely reverse *MYCN*-driven chemoresistance and re-sensitize tumors to platinum-based chemotherapy. These results provide a genotype-specific strategy to target a subset of chemoresistant SCLC that could potentially ultimately be applied in a clinical setting.

**5.2 Development of Engineered PDX Models**

One of the major strengths of our study is the development of a novel method using lentiviral infection to engineer stable PDX models of SCLC harboring single gene

perturbations. Previous studies of SCLC chemoresistance have relied on assessment of the genetic composition of unmodified PDX tumors following extended periods of treatment with platinum-based chemotherapy (Gardner 2017). A major drawback of this approach is the inability to draw deterministic conclusions about the roles of genes that were found to be deleteriously mutated in tumors post-treatment, as there is no way to tell at what stage or in what context said mutations arose. However, our approach allowed us to directly assess the effects of overexpression of specific oncogenes such as *MYCN* and *MYCL* on the development of cis-eto resistance by comparison to a matched control in an otherwise identical, chemosensitive system. Reducing cell culture time was a critical aspect of our novel approach to genetically perturb PDX models of SCLC, as it has been shown that PDX models passaged in vivo more fully recapitulate the expression of the original tumor vs. derived cell lines (Daniel 2009). While our earliest experiments initially employed a 16 hour culture period for lentiviral infections (Fig. 2.2, 2.3, 3.2, 3.4), our current protocols reduce the time in ex vivo culture to under 4 hours (Fig. 2.7, 3.5). Moreover, using the two-step system for model propagation outlined in Chapter 2, we can generate single gene perturbed PDX models that can be cryopreserved, shared, and repropagated at any time for functional or therapeutic studies. Similar systems of engineering stable PDX models with single gene perturbations have shown promise as a platform to interrogate the functions of SCLC driver genes (Hulton 2020). As such, our method of designing and generating customized PDX models can form the backbone of future studies in the lab beyond those described in Chapters 2 and 3. Given that the response of GEM models to chemotherapy does not typically include the strong regressions often observed in

human SCLC patients, employment of chemosensitive PDX models that mimic the response of the originating patient are a critical tool for the SCLC field.

### 5.3 In Vivo CRISPR-Cas9 Screens Identify SAGA Complex Components as Potential Drivers of SCLC Chemoresistance

We utilized our modifiable, chemosensitive PDX system to perform in vivo functional CRISPR-Cas9 screens initially on a genome-wide scale and subsequently in a targeted, SCLC specific approach. Previous studies, including in our lab, have employed CRISPR-Cas9 screens to identify key driver genes in human SCLC cell lines as well as in cell lines derived from autochthonous mouse models of SCLC (Li 2019). Furthermore, while in vivo CRISPR-Cas9 screens have been conducted in models other tumor types, the only published in vivo screen of SCLC to date is a recent study that utilized an adenoviral vector system containing a CRISPR-Cas9 sgRNA library to infect cohorts of *RP* mice with the goal of identifying drivers of SCLC in the absence of any treatment (Ng 2020). As such, our study demonstrates the first known comprehensive in vivo CRISPR-Cas9 screen designed to identify drivers of chemoresistance in SCLC. As the FHSC14 PDX model was derived in house from a chemonaive patient and is highly chemosensitive at baseline (Augert 2019), it is an ideal system in which to study genes whose inactivation may play a role in the development of chemoresistance.

Upon performing screens using our Focused SCLC library, we identified numerous potential candidate genes for future validation as drivers of SCLC chemoresistance. Most notable were genes such as *USP22, TADA1*, and *TAF5L* that code for members of the Spt-Ada-Gcn5 acetyltransferase (SAGA) complex. Guides targeting these genes,

particularly *USP22*, were found to be significantly enriched in cis-eto treated tumors across multiple modes of analysis in multiple screens, including the initial genome-wide screen. The SAGA complex is a large multi-subunit complex that is composed of numerous effector modules including a histone acetyltransferase (HAT) and deubiquitinase (DUB) domain (Han 2014). The SAGA complex is known to interact with and share components with several other complexes such as the ATAC and TFIID complexes (Helmlinger 2017). As such, the SAGA complex and many of its constituent members play important roles in the regulation of key processes such as gene transcription, nucleosome remodeling, and histone deubiquitination among others (Han 2014, Morgan 2016, Helmlinger 2017). Furthermore, many of the components of the SAGA complex have been described as essential genes (Han 2014). In the context of cancer, *USP22*, the key effector of the SAGA DUB module, has been shown to act as an oncogene and promote tumor progression in several cancers including NSCLC (Ding 2014, Schrecengost 2014, Hu 2015, Xiao 2015). Furthermore, overexpression of *USP22* has been shown to be correlated with therapeutic resistance, including for cisplatin, in several cell line based studies of hepatocellular carcinoma and NSCLC (Ling 2017, Wang 2017, Yun 2018). However, *USP22* and the SAGA complex as a whole have never been extensively studied in SCLC and the results of our screens described in Chapter 3 suggest conversely that loss of SAGA complex members may in fact promote chemoresistance. Future studies currently underway will focus on perturbing *USP22* and other SAGA complex genes in our chemosensitive PDX models to determine if loss of these genes can confer chemoresistance. Additionally, ongoing future experiments include additional in vivo CRISPR-Cas9 screens using Focused

SCLC library in 3 additional chemosensitive PDX models. As such, the tools and systems engineered as part of this study will form the basis for a platform of broad, comprehensive studies aimed at identifying drivers of chemoresistance in SCLC.

## References


Augert, A., Eastwood, E., Ibrahim, A.H., Wu, N., Grunblatt, E., Basom, R., et al (2019). "Targeting NOTCH activation in small cell lung cancer through LSD1 inhibition." Sci Signal **12**(567): eaau2922.

Augert, A., Zhang, Q., Bates, B., Cui, M., Wang, X., Wildey, G., et al (2017). "Small cell lung cancer exhibits frequent inactivating mutations in the histone methyltransferase KMT2D/MLL2: CALGB 151111 (Alliance)." J Thorac Oncol **12**(4): 704-713.

Beronja, S., Livshits, G., William, S., Fuchs, E. (2010). "Rapid functional dissection of genetic networks via tissue-specific transduction and RNAi in mouse embryos." Nat Med **16**(7): 821-827.

Borromeo, M. D., Savage, T.K., Kollipara, R.K., He, M., Augustyn, A., Osborne, J.K., et al (2016). "ASCL1 and NEUROD1 reveal heterogeneity in pulmonary neuroendocrine tumors and regulate distinct genetic programs." Cell Rep **16**(5): 1259-1272.

Bottger, F., Semenova, E.A., Song, J.Y., Ferone, G., van der Vilet, J., Cozijnsen, M., et al (2019). "Tumor heterogeneity underlies differential cisplatin sensitivity in mouse models of small cell lung cancer." Cell Rep **27**: 3345-3358.

Brennan, J., O'Connor, T., Makuch, R.W., Simmons, A.M., Russell, E., Linnoila, R.I., et al (1991). "myc family DNA amplification in 107 tumors and tumor cell lines from patients with small cell lung cancer treated with different combination chemotherapy regimens." Cancer Res **51**(6): 1708-1712.

Bunn, P. A., Minna, J.D., Augustyn, A., Gazdar, A.F., Ouadah, Y., Krasnow, M.A., et al (2016). "Small cell lung cancer: can recent advances in biology and molecular biology be translated into improved outcomes." J Thorac Oncol **11**(4): 453-474.

Byers, L. A., Rudin, C.M. (2015). "Small cell lung cancer, where do we go from here?" Cancer **121**(5): 664-672.

Carney, D. N., Gazdar, A.F., Bepler, G., Guccion, J.G., Marangos, P.J., Moody, T.W., et al (1985). "Establishment and identification of small cell lung cancer cell lines having classic and variant features." Cancer Res **45**(6): 2913-2923.

Chen, S., Sanjana, N.E., Zheng, K., Shalem, O., Lee, K., Shi, X., et al (2015). "Genome-wide CRISPR screen in a mouse model of tumor growth and metastasis." Cell **160**(6): 1246-1260.

Chow, R. D., Chen, S. (2018). "Cancer CRISPR screens in vivo." Trends Cancer **4**(5): 349-358.

Cong, L., Ran, F.A., Cox, D., Lin, S., Barretto, R., Habib, N., et al (2013). "Multiplex genome engineering using CRISPR/Cas9 systems." Science **339**: 819-823.

Cui, M., Augert, A., Rongione, M., Conkrite, K., Parazzoli, S., Nikitin, A.Y., et al (2014). "PTEN is a potent suppressor of small cell lung cancer." Mol Cancer Res **12**(5): 654-659.

Daniel, V. C., Marchionni, L., Hierman, J.S., Rhodes, J.T., Devereux, W.L., Rudin, C.M. (2009). "A primary xenograft model of small cell lung cancer reveals irreversible changes in gene expression imposed by culture in vitro." Cancer Res **69**(8): 3364-3373.

Ding, F., Bao, C., Tian, Y., Xiao, H., Wang, M., Xie, X., et al (2014). "USP22 promotes NSCLC tumorigenesis via MDMX up-regulation and subsequent p53 inhibition." Int J Mol Sci **16**(1): 307-320.

Dooley, A. L., Winslow, M.M., Chiang, D.Y., Banerji, S., Stransky, N., Dayton, T.L., et al (2011). "Nuclear factor I/B is an oncogene in small cell lung cancer." Genes Dev **25**(14): 1470-1475.

Drapkin, B. J., George, J., Christensen, C.L., Mino-Kenudson, M., Dries, R., Sundaresan, T., et al (2018). "Genomic and functional fidelity of small cell lung cancer patient derived xenografts." Cancer Discov **8**(5): 600-615.

DuPage, M., Dooley, A.L., Jacks, T. (2009). "Conditional mouse lung cancer models using adenoviral or lentiviral delivery of Cre recombinase." Nat Protoc **4**(7): 1064-1072.

Evers, B., Jastrzebski, K., Heijmans, J.P., Grernum, W., Beijersbergen, R.L., Bernards, R. (2016). "CRISPR knockout screening outperforms shRNA and CRISPRi in identifying essential genes." Nat Biotechnol **34**(6): 631-633.

Gardner, E. E., Lok, B.H., Schneeberger, V.E., Desmeules, P., Miles, L.A., Arnold, P.K., et al (2017). "Chemosensitive relapse in small cell lung cancer proceeds through an EZH2-SLFN11 axis." Cancer Cell **31**(2): 286-299.

Gazdar, A. F., Carney, D.N., Russell, E.K., Sims, H.L., Baylin, S.B., Bunn, P.A., et al (1980). "Establishment of continuous, clonable cultures of small cell carcinoma of lung which have amine precursor uptake and decarboxylation cell properties." Cancer Res **40**(10): 3502-3507.

George, J., Lim, J.S., Jang, S.J., Cun, Y., Ozretic, L., Kong, G., et al (2015). "Comprehensive genomic profiles of small cell lung cancer." Nature **524**(7563): 47-53.

Han, K., Pierce, S.E., Li, A., Spees, K., Anderson, G.R., Seoane, J.A., et al (2020). "CRISPR screens in cancer spheroids identify 3D growth-specific vulnerabilities." Nature **580**(7801): 136-141.

Han, Y., Luo, J., Ranish, J., Hahn, S. (2014). "Architecture of the Saccharomyces cerevisiae SAGA transcription coactivator complex." EMBO J **22**(21): 2534-2546.

Helmlinger, D., Tora, L. (2017). "Sharing the SAGA." Trends Biochem Sci **42**(11): 850-861.

Hodgkinson, C. L., Morrow, C.J., Li, Y., Metcalf, R.L., Rothwell, D.G., Trapani, F., et al (2014). "tumorigenicity and genetic profiling of circulating tumor cells in small cell lung cancer." Nat Med **20**(8): 897-903.

Horn, L., Mansfield, A.S., Szczesna, A., Havel, L., Krzakowski, M., Hochmair, M.J., et al (2018). "First-line atezolizumab plus chemotherapy in extensive stage small cell lung cancer." N Engl J Med **379**(23): 2220-2229.

Hou, P., Wu, C., Wang, Y., Qi, R., Bhavanasi, D., Zuo, Z., et al (2017). "A Genome-Wide CRISPR Screen Identifies Genes Critical for Resistance to FLT3 Inhibitor AC220." Cancer Res **77**(16): 4402-4413.

Hsu, P. D., Lander, E.S., Zhang, F. (2014). "Development and applications of CRISPR-Cas9 for genome engineering." Cell **157**(6): 1262-1278.

Hu, J., Yang, D., Zhang, H., Liu, W., Zhao, Y., Lu, H., et al (2015). "USP22 promotes tumor progression and induces epithelial-mesenchymal transition in lung adenocarcinoma." Lung Cancer **88**(3): 239-245.

Huang, Y. H., Klingbeil, O., He, X.Y., Wu, X.S., Arun, G., Lu, B., et al (2018). "POU2F3 is a master regulator of a tuft cell like variant of small cell lung cancer." Genes Dev **32**(13-14): 915-928.

Huijbers, I. J., Bin Ali, R., Pritchard, C., Cozijnsen, M., Kwon, M.C., Proost, N., et al (2014). "Rapid target gene validation in complex cancer mouse models using re-derived embryonic stem cells." EMBO Mol Med **6**(6): 212-225.

Hulton, C. H., Costa, E.A., Shah, N.S., Quintanal-Villalonga, A., Heller, G., de Stanchina, E., et al (2020). "Direct genome editing of patient-derived xenografts using CRISPR-Cas9 enables rapid in vivo functional genomics." Nat Cancer **1**: 359-369.

Iwakawa, R., Kohno, T., Totoki, Y., Shibata, T., Tsuchihara, K., Mimaki, S., et al (2015). "Expression and clinical significance of genes frequently mutated in small cell lung cancers defined by whole exome/RNA sequencing." Carcinogenesis **36**(6): 616-621.

Jia, D., Augert, A., Kim, D.W., Eastwood, E., Wu, N., Ibrahim, A.H., et al (2018). "Crebbp loss drives small cell lung cancer and increases sensitivity to HDAC inhinbition." Cancer Discov **8**(11): 1422-1437.

Jinek, M., Chylinski, K., Fonfara, I., Hauer, M., Doudna, J.A., Charpentier, E. (2012). "A programmable dual RNA guided DNA endonuclease in adaptive bacterial immunity." Science **337**: 816-821.

Johnson, B. E., Ihde, D.C., Makuch, R.W., Gazdar, A.F., Carney, D.N., Oie, H., et al (1987). "Myc family oncogene amplification in tumor cell lines established from small cell lung cancer patients and its relationship to clinical status and course." J Clin Invest **79**(6): 1629-1634.

Kato, F., Fiorentino, F.P., Alibes, A., Perucho, M., Sanchez-Cespedes, M., Kohno, T., et al (2016). "MYCL is a target of a BET bromodomain inhibitor, JQ1, on growth suppression efficacy in small cell lung cancer cells." Oncotarget **7**(47): 77378-77388.

Kim, D. W., Wu, N., Kim, Y.C., Cheng, P.F., Basom, R., Kim, D., et al (2016). "Genetic requirement for Mycl and efficacy of RNA pol I inhibition in mouse models of small cell lung cancer." Genes Dev **30**(11): 270-285.

Lallo, A., Frese, K.K., Morrow, C.J., Sloane, R., Gulati, S., Schenk, M.W., et al (2018). "The combination of the PARP inhibitor Olaparib and the WEE1 inhibitor AZD1775 as a new therapeutic option for small cell lung cancer." Clin Cancer Res **24**(20): 5153-5164.

Langmead, B., Trapnell, C., Pop, M., Salzberg, S.L. (2009). "Ultrafast and memory efficient alignment of short DNA sequences to the human genome." Genome Biol **10**: R25.

Leinhart, R., Kirov, S., Desilva, H., Cao, J., Lei, M., Johnston, K., et al (2015). "Sensitivity of small cell lung cancer to BET inhibition is mediated by regulation of ASCL1 gene expression." Mol Cancer Ther **14**(10): 2167-2174.

Li, L., Ng, S.R., Colon, C.I., Drapkin, B.J., Hsu, P.P., Li, Z., et al (2019). "Identification of DHODH as a therapeutic target in small cell lung cancer." Sci Transl Med **11**(517): eaaw7852.

Li, W., Koster, J., Xu, H., Chen, C.H., Xiao, T., Liu, J.S., et al (2015). "Quality control, modeling, and visualization of CRISPR screens with MAGeCK-VISPR." Genome Biol **16**: 281.

Li, W., Xu, H., Xiao, T., Cong, L., Love, M.I., Zhang, F., et al (2014). "MAGeCK enables robust identification of essential genes from genome-scale CRISPR\Cas9 knockout screens." Genome Biol **15**(12): 554.

Ling, S., Li, J., Shan, Q., Dai, H., Lu, D., Wen, X., et al (2017). "USP22 mediates the multidrug resistance of hepatocellular carcinoma via the SIRT1/AKT/MRP1 signaling pathway." Mol Oncol **11**(6): 682-695.

Mali, P., Yang, L., Esvelt, K.M., Aach, J., Guell, M., DiCarlo, J.E., et al (2013). "RNA guided human genome engineering via Cas9." Science **339**: 823-826.

Manguso, R. T., Pope, H.W., Zimmer, M.D., Brown, F.D., Yates, K.B., Miller, B.C., et al (2017). "In vivo CRISPR screening identifies Ptpn2 as a cancer immunotherapy target." Nature **547**(7664): 413-418.

McKoll, K., Wildey, G., Sakre, N., Lipka, M.B., Behtaj, M., Kresak, A., et al (2017). "Reciprocal expression of INSM1 and YAP1 defines subgroups in small cell lung cancer." Oncotarget **28**(8): 73745-73756.

Meier, J. A., Zhang, F., Sanjana, N.E. (2017). "GUIDES: sgRNA design for loss-of-function screens." Nat Methods **14**(9): 831-832.

Meuwissen, R., Linn, S.C., Linnoila, R.I., Zevenhoven, J., Mooi, W.J., Berns, A. (2003). "Induction of small cell lung cancer by somatic inactivation of both Trp53 and Rb1 in a conditional mouse model." Cancer Cell **4**(3): 181-189.

Mollaoglu, G., Guthrie, M.R., Bohm, S., Bragelmann, J., Can, I., Ballieu, P.M., et al (2017). "MYC drives progression of small cell lung cancer to a variant neuroendocrine subtype with vulnerability to aurora kinase inhibition." Cancer Cell **31**(2): 270-285.

Morgan, M. T., Haj-Yahya, M., Ringel, A.E., Bandi, P., Brik, A., Wolberger, C. (2016). "Structural basis for histone H2B deubiquitination by the SAGA DUB module." Science **351**: 725-728.

Ng, S. R., Rideout, W.M., Akama-Garren, E.H., Bhutkar, A., Mercer, K.L., Schenkel, J.M., et al (2020). "CRISPR-mediated modeling and functional validation of candidate tumor suppressor genes in small cell lung cancer." Proc Natl Acad Sci U.S.A. **117**(1): 513-521.

Oser, M. G., Niederst, M.J., Sequist, L.V., Engelman, J.A. (2015). "Transformation from non-small-cell lung cancer to small-cell lung cancer: molecular drivers and cells of origin." Lancet Oncol **16**(4): 165-172.

Pacheco, J., Bunn, P.A. (2019). "Advancements in small cell lung cancer: the changing landscape following Impower-133." Clin Lung Cancer **20**(3): 148-160.

Park, K. S., Liang, M.C., Raiser, D.M., Zamponi, R., Roach, R.R., Curtis, S.J. (2011). "Characterization of the cell of origin for small cell lung cancer." Cell Cycle **10**(16): 2806-2815.

Paz-Ares, L., Dvorkin, M., Chen, Y., Reinmuth, N., Hotta, K., Trukhin, D., et al (2019). "Durvalumab plus platinum-etoposide versus platinum-etoposide in first-line treatment of extensive stage small cell lung cancer (CASPIAN): a randomized, controlled, open label, phase 3 trial." Lancet **394**(10212): 1929-1939.

Peifer, M., Fernandez-Cuesta, L., Sos, M.L., George, J., Seidel, D., Kasper, L.H., et al (2012). "Integrative genomic analyses identify key somatic driver mutations of small cell lung cancer." Nat Genet **44**: 1104-1110.

Pelish, H. E., Liau, B.B., Nitulescu, I.I., Tangpeerachaikul, A., Poss, Z.C., Da Silva, D.H., et al (2015). "Mediator kinase inhibition further activates super-enhancer-associated genes in AML." Nature **526**(7572): 273-276.

Phelps, R. M., Johnson, B.E., Ihde, D.C., Gazdar, A.F., Carbone, D.P., McClintock, P.R., et al (1996). "NCI-Navy medical oncology branch cell line data base." J Cell Biochem Suppl **24**: 32-91.

Poirier, J. T., George, J., Owonikoko, T.K., Berns, A., Brambilla, E., Byers, L.A., et al (2020). "New approaches to SCLC therapy: from the laboratory to the clinic." J Thorac Oncol **15**(4): 520-540.

Rossi, A., Di Maio, M., Chiodini, P., Rudd, R.M., Okamoto, H., Skarlos, D.V., et al (2012). "Carboplatin or cisplatin based chemotherapy in first line treatment of small cell lung cancer: the COCIS meta-analysis of individual patient data." J Clin Oncol **30**(14): 1692-1698.

Rudin, C. M., Durinck, S., Stawiski, E.W., Poirier, J.T., Modrusan, Z., Shames, D.S., et al (2012). "Comprehensive genomic analysis identifies SOX2 as a frequently amplified gene in small cell lung cancer." Nat Genet **44**(10): 1111-1116.

Rudin, C. M., Poirier, J.T., Byers, L.A., Dive, C., Dowlati, A., George, J., et al (2019). "Molecular subtypes of small cell lung cancer: a synthesis of human and mouse model data." Nat Rev Cancer **19**(5): 289-297.

Ruiz, S., Mayor-Ruiz, C., Lafarga, V., Murga, M., Vega-Sendino, M., Ortega, S., et al (2016). "A Genome-wide CRISPR Screen Identifies CDC25A as a Determinant of Sensitivity to ATR Inhibitors." Mol Cell **62**(2): 307-313.

Sanchez-Rivera, F. J., Jacks, T. (2015). "Applications of the CRISPR-Cas9 system in cancer biology." Nat Rev Cancer **15**(7): 387-395.

Sanjana, N. E., Shalem, O., Zhang, F. (2014). "Improved vectors and genome-wide libraries for CRISPR screening." Nat Methods **11**(8): 783-784.

Schaffer, B. E., Parks, K.S., Yiu, G., Conklin, J.F., Lin, C., Burkhart, D.L., et al (2010). "Loss of p130 accelerates tumor development in a mouse model for human small cell lung carcinoma." Cancer Res **70**(10): 3877-3883.

Schrecengost, R. S., Dean, J.L., Goodwin, J.F., Schiewer, M.J., Urban, M.W., Stanek, T.J., et al (2014). "USP22 regulates oncogenic signaling pathways to drive lethal cancer progression." Cancer Res **74**(1): 272-286.

Sen, T., Tong, P., Diao, L., Li, L., Fan, Y., Hoff, J., et al (2017). "Targeting AXL and mTOR pathway overcomes primary and acquired resistance to WEE1 inhibition in small cell lung cancer." Clin Cancer Res **23**(20): 6239-6253.

Shalem, O., Sanjana, N.E., Hartenian, E., Shi, X., Scott, D.A., Mikkelson, T., et al (2014). "Genome-scale CRISPR-Cas9 knockout screening in human cells." Science **343**: 84-87.

Shalem, O., Sanjana, N.E., Zhang, F. (2015). "High-throughput functional genomics using CRISPR-Cas9." Nat Rev Genet **16**(5): 299-311.

Sutherland, K. D., Proost, N., Brouns, I., Adriansen, D., Song, J.Y., Berns, A. (2011). "Cell of origin of small cell lung cancer: inactivation of Trp53 and Rb1 in distinct cell types of adult mouse lung." Cancer Cell **19**(6): 754-764.

Tavana, O., Li, D., Dai, C., Lopez, G., Banerjee, D., Kon, N., et al (2016). "HAUSP deubiquitinates and stabilizes N-Myc in neuroblastoma." Nat Med **22**(10): 1180-1186.

Wagner, A. H., Devarakonda, S., Skidmore, Z.L., Krysiak, K., Ramu, A., Trani, L., et al (2018). "Recurrent WNT pathway alterations are frequent in relapsed small cell lung cancer " Nat Commun **9**(1): 3787.

Wang, A., Ning, Z., Lu, C., Gao, W., Liang, J., Yan, Q., et al (2017). "USP22 Induces Cisplatin Resistance in Lung Adenocarcinoma by Regulating γH2AX-Mediated DNA Damage Repair and Ku70/Bax-Mediated Apoptosis." Front Pharmacol **8**: 274.

Wang, T., Birsoy, K., Hughes, N.W., Krupczak, K.M., Post, Y., Wei, J.J., et al (2015). "Identification and characterization of essential genes in the human genome." Science **350**: 1096-1101.

Wang, T., Wei, J.J., Sabatini, D.M., Lander, E.S. (2014). "Genetic screens in human cells using the CRISPR-Cas9 system." Science **343**: 80-84.

Wang, T., Yu, H., Hughes, N.W., Liu, B., Kendirli, A., Klein, K., et al (2017). "Gene Essentiality Profiling Reveals Gene Networks and Synthetic Lethal Interactions with Oncogenic Ras." Cell **168**(5): 890-903.

Xiao, H., Tian, Y., Yang, Y., Hu, F., Xie, X., Mei, J., et al (2015). "USP22 acts as an oncogene by regulating the stability of cyclooxygenase-2 in non-small cell lung cancer." Biochem Biophys Res Commun **460**(3): 703-708.

Yang, D., Denny, S.K., Greenside, P.G., Chaikovsky, A.C., Brady, J.J., Ouadah, Y., et al (2018). "Intertumoral Heterogeneity in SCLC Is Influenced by the Cell Type of Origin." Cancer Discov **8**(10): 1316-1331.

Yang, X., Boehm, J.S., Yang, X., Salehi-Ashtiani, K., Hao, T., Shen, Y., et al (2011). "A public genome-scale lentiviral expression library of human ORFs." Nat Methods **8**(8): 659-661.

Yun, X., Zhang, K., Wang, J., Pangeni, R.P., Yang, L., Bonner, M., et al (2018). "Targeting USP22 Suppresses Tumorigenicity and Enhances Cisplatin Sensitivity Through ALDH1A3 Downregulation in Cancer-Initiating Cells from Lung Adenocarcinoma." Mol Cancer Res **16**(7): 1161-1171.

## Appendix

**Table A.1: Genes enriched in Genome-wide FHSC14 screen: Saline Pool.** Table listing all genes found to have either 5 or 6 corresponding sgRNAs enriched in the Saline Pool relative to the P0.

| 5 sgRNAs Enriched | 6 sgRNAs Enriched |
|---|---|
| EFCAB1 | ADRB2 |
| EMILIN3 | C15orf59 |
| ACTR1A | C8orf74 |
| AK1 | CD38 |
| ANHX | CHST2 |
| ANLN | CRKL |
| ARHGEF18 | D2HGDH |
| ARPC1A | FAM63B |
| ARPC5L | HN1L |
| ASB10 | IZUMO2 |
| ASB7 | KLHL25 |
| AVIL | LDOC1L |
| AXDND1 | MPP4 |
| B9D1 | MPV17 |

| | |
|---|---|
| BAALC | MS4A2 |
| BAG4 | PLEKHA8 |
| BICC1 | PRDM11 |
| C13orf35 | TBCK |
| C15orf43 | TMEM42 |
| C1orf116 | |
| C5AR2 | |
| CA2 | |
| CABLES1 | |
| CASC4 | |
| CASP10 | |
| CCDC109B | |
| CCDC146 | |
| CCDC179 | |
| CCDC81 | |
| CCDC85A | |
| CD163 | |
| CERKL | |
| CH25H | |
| CHMP1A | |
| CHRNA5 | |
| CISD3 | |
| CLDN8 | |
| CLIP4 | |
| CLSTN1 | |
| CPNE5 | |
| CREB3L4 | |
| CS | |
| CSF1R | |
| CXCL9 | |
| DBI | |
| DCAF8L2 | |
| DCD | |
| DDX58 | |
| DHRS4L1 | |
| DIABLO | |
| DNAJC21 | |
| ECHDC2 | |
| ECT2L | |
| EEF2K | |
| EMC8 | |
| EMP3 | |
| EPHB1 | |

| | |
|---|---|
| ERAS | |
| ERGIC3 | |
| ETV4 | |
| FABP1 | |
| FAM177A1 | |
| FAM220A | |
| FAM9C | |
| FGFR2 | |
| FHOD1 | |
| FKBP9 | |
| FOCAD | |
| FOXB1 | |
| FUT5 | |
| FZD7 | |
| GBP3 | |
| GDF3 | |
| GGT6 | |
| GIMAP5 | |
| GLCCI1 | |
| GLIPR1L1 | |
| GNL3L | |
| GNRH2 | |
| GPR133 | |
| GPR137B | |
| GPR37 | |
| GPR61 | |
| HAS1 | |
| HBP1 | |
| HDAC11 | |
| HIPK4 | |
| HIST4H4 | |
| HMGCS2 | |
| HNRNPR | |
| HOXA5 | |
| HPN | |
| HS3ST6 | |
| IDI2 | |
| IFNA6 | |
| IFNG | |
| IGF2BP3 | |
| IGFBP7 | |
| IGSF5 | |
| ITGAD | |

| | |
|---|---|
| ITGAM | |
| KCNAB3 | |
| KCNJ6 | |
| KDM1A | |
| KIAA1109 | |
| KIAA1191 | |
| KIAA1407 | |
| KIAA1432 | |
| KIAA1598 | |
| KIF3A | |
| KLHL24 | |
| KLLN | |
| KRTAP12-3 | |
| KRTAP20-2 | |
| KRTAP5-4 | |
| KSR1 | |
| LAYN | |
| LCE2C | |
| LCNL1 | |
| LHFPL4 | |
| LMAN1 | |
| LPAR6 | |
| LRRC31 | |
| LRRIQ4 | |
| LTB4R2 | |
| LTC4S | |
| LYAR | |
| LYG2 | |
| MAFK | |
| MAP1LC3B2 | |
| METTL23 | |
| METTL9 | |
| MGAM | |
| MMP16 | |
| MPPED1 | |
| MRC2 | |
| MROH7 | |
| MS4A7 | |
| MSN | |
| MUC22 | |
| MUM1L1 | |
| MX1 | |
| MYH11 | |

| | |
|---|---|
| NAA60 | |
| NAV3 | |
| NCOA6 | |
| NDRG4 | |
| NMUR1 | |
| NOXA1 | |
| NPW | |
| NXF5 | |
| ODF3B | |
| OR2C1 | |
| OR4K13 | |
| OR52A1 | |
| OR52E2 | |
| OR6Q1 | |
| OR9Q2 | |
| ORC1 | |
| PARVB | |
| PATE4 | |
| PCDH15 | |
| PCYOX1 | |
| PDCD6IP | |
| PDE4B | |
| PDK3 | |
| PIH1D2 | |
| PPIC | |
| PPME1 | |
| PRADC1 | |
| PRAMEF12 | |
| PROL1 | |
| PRSS36 | |
| PSD2 | |
| PSG6 | |
| PVRL4 | |
| RAB3IP | |
| RAET1G | |
| RANBP6 | |
| RGMA | |
| RIMS1 | |
| RLBP1 | |
| RRAGA | |
| S100G | |
| SAMD11 | |
| SDF4 | |

| | |
|---|---|
| SEC14L6 | |
| SERPINA9 | |
| SH3D19 | |
| SIPA1L3 | |
| SIRT6 | |
| SKOR1 | |
| SLC10A1 | |
| SLC22A11 | |
| SLC22A13 | |
| SLC22A16 | |
| SLC25A11 | |
| SLC37A4 | |
| SLC51B | |
| SLC5A5 | |
| SLC7A14 | |
| SLPI | |
| SNRNP70 | |
| SNX18 | |
| SPATA31A6 | |
| SPNS2 | |
| SRSF12 | |
| SSC5D | |
| SSTR4 | |
| STAMBP | |
| STK10 | |
| STK39 | |
| SULT1E1 | |
| SYTL5 | |
| TAGAP | |
| TAS2R4 | |
| TASP1 | |
| TCP11L1 | |
| TEC | |
| TENM2 | |
| THBS2 | |
| THNSL2 | |
| TIA1 | |
| TMEM215 | |
| TNFRSF10C | |
| TRABD2A | |
| TRIM71 | |
| TSNAX | |
| TUSC3 | |

| | |
|---|---|
| UBA2 | |
| UQCR11 | |
| WASL | |
| WFIKKN1 | |
| XKR8 | |
| XKRY | |
| YWHAE | |
| ZC3H12A | |
| ZDHHC14 | |
| ZFP36 | |
| ZMAT3 | |
| ZNF101 | |
| ZNF117 | |
| ZNF17 | |
| ZNF18 | |
| ZNF229 | |
| ZNF24 | |
| ZNF26 | |
| ZNF280D | |
| ZNF414 | |
| ZNF454 | |
| ZNF517 | |
| ZNF703 | |
| ZNF713 | |
| ZNF749 | |
| ZNF827 | |
| ZP1 | |
| ZSCAN1 | |

**Table A.2: Genes enriched in Genome-wide FHSC14 screen: Cis-Eto Pool.** Table listing all genes found to have either 5 or 6 corresponding sgRNAs enriched in the Cis-Eto Pool relative to the P0.

| 4 sgRNAs Enriched | 5 sgRNAs Enriched |
|---|---|
| ABAT | APMAP |
| ACOT4 | ARPC5L |
| ALDH3A1 | CCDC34 |
| ANKS1A | CDC34 |
| AQP9 | CELF5 |
| ARNT2 | DLEU7 |

| | |
|---|---|
| ATHL1 | DLX3 |
| ATP6V0A2 | FOXJ1 |
| B3GALT2 | FZD3 |
| B3GALT5 | IFNA7 |
| B4GALT4 | ITPRIP |
| BCAR1 | POGK |
| BHLHE40 | SFXN2 |
| BLK | SHC2 |
| BRD9 | SMG9 |
| C14orf39 | STIP1 |
| C17orf51 | TOP3B |
| C1orf27 | TRMT11 |
| C1QBP | USP22 |
| C22orf15 | WDR49 |
| C2CD4A | YIPF7 |
| C6orf70 | ZMYM2 |
| C8orf48 | ZNF319 |
| CACNG8 | ZNF485 |
| CADM1 | |
| CALML5 | |
| CASP6 | |
| CASP7 | |
| CCDC129 | |
| CCDC180 | |
| CCDC42B | |
| CD3E | |
| CDKL5 | |
| CDKN2AIPNL | |
| CHRM4 | |
| CLDN11 | |
| CMTM4 | |
| COG7 | |
| CORO1B | |
| CPEB3 | |
| CPLX2 | |
| CPN1 | |
| CPN2 | |
| CPT1A | |
| CYBB | |
| CYP27A1 | |
| DALRD3 | |
| DAPL1 | |
| DBNL | |

| | |
|---|---|
| DCAF16 | |
| DCAF8L1 | |
| DESI2 | |
| DLC1 | |
| DNMT3B | |
| DTD2 | |
| DYNLL2 | |
| EIF1AY | |
| ELANE | |
| EPO | |
| ESRP2 | |
| FABP2 | |
| FAHD2B | |
| FAM127B | |
| FAM151A | |
| FAM47A | |
| FAM90A1 | |
| FAS | |
| FASTK | |
| FHL3 | |
| FOXH1 | |
| FSHB | |
| FUT3 | |
| GAB4 | |
| GAL3ST1 | |
| GP6 | |
| GRHL1 | |
| GSG1L | |
| GSTM5 | |
| HAGH | |
| HESX1 | |
| HFE2 | |
| HHIPL2 | |
| HIST1H3A | |
| HIST1H3C | |
| HIST1H4L | |
| HLA-DRB1 | |
| HLA-G | |
| HNRNPA1 | |
| HOXD4 | |
| HS2ST1 | |
| hsa-mir-144 | |
| hsa-mir-300 | |

| | |
|---|---|
| hsa-mir-3653 | |
| hsa-mir-4311 | |
| hsa-mir-4639 | |
| hsa-mir-571 | |
| hsa-mir-6771 | |
| HTR1F | |
| HYOU1 | |
| ICAM4 | |
| IFITM10 | |
| IFNGR1 | |
| IFT122 | |
| IGFBP1 | |
| IL7R | |
| KCNIP3 | |
| KCTD19 | |
| KIAA1377 | |
| KLHDC3 | |
| KLK5 | |
| KLRF2 | |
| KRTAP25-1 | |
| KRTAP3-3 | |
| LAPTM5 | |
| LCE2D | |
| LCNL1 | |
| LDHD | |
| LGALS1 | |
| LGALS14 | |
| LPAR6 | |
| MAB21L2 | |
| MAP3K11 | |
| ME1 | |
| MECR | |
| MED16 | |
| MED24 | |
| MID1 | |
| MMP26 | |
| MPPED1 | |
| MRGPRX3 | |
| MRPS12 | |
| MS4A7 | |
| MTA2 | |
| MTRNR2L4 | |
| MYH7B | |

| | |
|---|---|
| NCKAP1L | |
| NLRX1 | |
| NME6 | |
| NOS1 | |
| NPR1 | |
| NPR2 | |
| NR1H4 | |
| NRAP | |
| NRBF2 | |
| NT5C2 | |
| NUDT10 | |
| NYAP2 | |
| ODC1 | |
| OFD1 | |
| OLFML2B | |
| OPN4 | |
| OR2F1 | |
| OR3A2 | |
| OR7C2 | |
| OTUD6A | |
| OTUD6B | |
| OTUD7B | |
| P2RX2 | |
| P2RY8_Y | |
| PDGFRB | |
| PER1 | |
| PFKL | |
| PIGG | |
| PLEKHB1 | |
| POU3F2 | |
| PPP6R3 | |
| PRR18 | |
| PTHLH | |
| PTTG2 | |
| PWWP2B | |
| RAB33A | |
| RAB8B | |
| RALYL | |
| RBPJ | |
| RMND5B | |
| RNASE8 | |
| RNASE9 | |
| RND2 | |

| | |
|---|---|
| SAGE1 | |
| SCML1 | |
| SEMA6C | |
| SERPINB13 | |
| SKOR1 | |
| SLC11A2 | |
| SLC16A14 | |
| SLC25A1 | |
| SLC25A16 | |
| SLC25A53 | |
| SLCO1C1 | |
| SPATA17 | |
| SPATA6L | |
| SPEF1 | |
| SPRED2 | |
| SPRED3 | |
| SRPK1 | |
| ST3GAL5 | |
| STK4 | |
| STRC | |
| STX17 | |
| SYBU | |
| TADA1 | |
| TAF5L | |
| TCF25 | |
| TCF4 | |
| TESC | |
| TFPI2 | |
| TIGD1 | |
| TLR10 | |
| TMCO6 | |
| TMEM43 | |
| TMEM50A | |
| TMF1 | |
| TPRX1 | |
| TREX1 | |
| TREX2 | |
| TTC17 | |
| TTC31 | |
| UCP3 | |
| UNK | |
| USP17L10 | |
| VEGFC | |

| | |
|---|---|
| WDR27 | |
| WDR91 | |
| WIPF2 | |
| WNK4 | |
| YIPF6 | |
| ZC2HC1B | |
| ZCCHC24 | |
| ZFYVE27 | |
| ZMIZ2 | |
| ZMYND10 | |
| ZNF233 | |
| ZNF280B | |
| ZNF501 | |
| ZNF527 | |
| ZNF555 | |
| ZNF566 | |
| ZNF629 | |
| ZNF747 | |
| ZSCAN25 | |
| MICAL1 | |
| NSUN2 | |
| TKTL2 | |
| TRMT10B | |
| SRGAP1 | |

**Table A.3: Focused SCLC Library.** Complete list of 400 genes targeted in the Focused SCLC Library.

| GENE |
|---|
| AKT3 |
| ALDH3A1 |
| ALDOA |
| ALK |
| ALOX12B |
| AMER1 |
| ANKRD11 |
| ANKS1A |
| APC |
| APMAP |
| AQP9 |
| AR |

| |
|---|
| ARAF |
| ARID1A |
| ARID1B |
| ARID2 |
| ARID5B |
| ARNT2 |
| ARPC5L |
| ASXL1 |
| ATM |
| ATP6V1G3 |
| ATR |
| ATRX |
| ATXN7 |
| ATXN7L3 |
| AURKB |
| BAP1 |
| BAX |
| BBC3 |
| BBS4 |
| BCAR1 |
| BCL2L11 |
| BCOR |
| BLM |
| BRAF |
| BRCA2 |
| BRD9 |
| C2CD4A |
| CACNA1H |
| CACNG8 |
| CADM1 |
| CAMK2D |
| CAMSAP3 |
| CARM1 |
| CASP14 |
| CASP3 |
| CASP6 |
| CASP7 |
| CBFB |
| CBL |
| CBX3 |
| CCDC170 |
| CCDC34 |
| CCND2 |

| |
|---|
| CDC34 |
| CDCP1 |
| CDH1 |
| CDK6 |
| CDK8 |
| CDKN1A |
| CDKN1B |
| CDKN2A |
| CDKN2B |
| CDKN2C |
| CDKN2D |
| CELF5 |
| CHD8 |
| CHRM4 |
| CLDN1 |
| CLDN11 |
| CPN1 |
| CPN2 |
| CRABP2 |
| CREBBP |
| CSF1R |
| CSF2RB |
| CSNK1A1 |
| CTNNB1 |
| CUL3 |
| CUL5 |
| CXCL16 |
| CYB561D2 |
| CYP27A1 |
| CYSLTR2 |
| DAPL1 |
| DAXX |
| DBNL |
| DDR2 |
| DLC1 |
| DLEU7 |
| DLX3 |
| DNMT1 |
| DNMT3A |
| DNMT3B |
| DOK3 |
| DOT1L |
| DUSP4 |

| |
|---|
| DVL2 |
| EGFR |
| EIF1AY |
| ELANE |
| ENY2 |
| EP300 |
| EPHA3 |
| EPHA5 |
| EPHA7 |
| EPHB1 |
| ERBB3 |
| ERBB4 |
| ERCC4 |
| ESR1 |
| ESRP2 |
| ETV1 |
| ETV3 |
| FAH |
| FAM90A1 |
| FANCA |
| FAS |
| FAT1 |
| FBXW7 |
| FGFR1 |
| FGFR3 |
| FGFR4 |
| FHL3 |
| FLCN |
| FLT1 |
| FLT3 |
| FLT4 |
| FOXF2 |
| FOXH1 |
| FOXJ1 |
| FOXO1 |
| FOXP1 |
| FRAT1 |
| FTSJ3 |
| FZD1 |
| FZD3 |
| FZD7 |
| GAB4 |
| GATA3 |

| |
|---|
| GLI1 |
| GOT1 |
| GP6 |
| GPX3 |
| GRHL1 |
| GRIN2A |
| GSG1L |
| GSK3B |
| GSTM5 |
| HAGH |
| HEATR1 |
| HECW1 |
| HESX1 |
| HEXA |
| HGF |
| HHIPL2 |
| HIST1H3A |
| HIST1H4L |
| HMOX1 |
| HNF1A |
| HS2ST1 |
| HTR1F |
| HTR6 |
| HUS1B |
| HYOU1 |
| ICAM4 |
| IFNA7 |
| IGF1R |
| IGFBP1 |
| IKZF1 |
| IL7R |
| INHBA |
| INPP4A |
| INPP4B |
| IQGAP2 |
| IRS1 |
| IRS2 |
| ITPRIP |
| JAK1 |
| JAK2 |
| KAT2A |
| KAT2B |
| KCNA1 |

| |
|---|
| KCNIP3 |
| KDM5A |
| KDM5C |
| KDM6A |
| KDM6B |
| KDR |
| KEAP1 |
| KIT |
| KLF8 |
| KLK5 |
| KMT2A |
| KMT2B |
| KMT2C |
| KMT2D |
| KNSTRN |
| KRT27 |
| KRT33B |
| KRTAP25-1 |
| LAMA1 |
| LATS2 |
| LCE1D |
| LDHD |
| LGALS9 |
| LMO7 |
| LYN |
| MAP2K1 |
| MAP2K4 |
| MAP2K7 |
| MAP3K1 |
| MAP3K11 |
| MAP3K13 |
| MAX |
| MBOAT4 |
| MCM2 |
| MDC1 |
| MDM2 |
| MDM4 |
| MED12 |
| MED16 |
| MED23 |
| MED24 |
| MET |
| METTL14 |

| |
|---|
| METTL3 |
| MGA |
| MGAT5 |
| MID1 |
| MITF |
| MMP14 |
| MMP26 |
| MRM1 |
| MRPL14 |
| MSH2 |
| MSH6 |
| MST1R |
| MTOR |
| MUC1 |
| NBN |
| NCOR1 |
| NDUFV3 |
| NEGR1 |
| NELFB |
| NELL1 |
| NF1 |
| NFE2L2 |
| NKX3-1 |
| NME6 |
| NOP10 |
| NOTCH1 |
| NOTCH2 |
| NOTCH3 |
| NOTCH4 |
| NPM1 |
| NQO1 |
| NSD1 |
| NTRK1 |
| NTRK3 |
| OPN4 |
| OTC |
| OTOP3 |
| PALB2 |
| PARP1 |
| PBRM1 |
| PDCD1 |
| PDGFRA |
| PDGFRB |

| |
|---|
| PIGG |
| PIK3C2G |
| PIK3C3 |
| PIK3CA |
| PIK3CG |
| PIK3R1 |
| PLS3 |
| PMS1 |
| POGK |
| POLD1 |
| POLE |
| POU3F2 |
| PPARD |
| PPP1R11 |
| PPP1R12C |
| PPP3CC |
| PPP6R3 |
| PRDM1 |
| PRDM14 |
| PREX2 |
| PRF1 |
| PRICKLE1 |
| PRKCI |
| PSMA4 |
| PSMD6 |
| PTEN |
| PTGDR2 |
| PTPRD |
| PTPRS |
| PTPRT |
| RAB8B |
| RAC2 |
| RAD50 |
| RASA1 |
| RB1 |
| RBL1 |
| RBL2 |
| RBPJ |
| RET |
| RHOQ |
| RICTOR |
| RIPK1 |
| RNASE8 |

| |
|---|
| RNF138 |
| ROS1 |
| RPL22L1 |
| RPTOR |
| RUNX1 |
| S100G |
| SCML1 |
| SEMA6C |
| SENP2 |
| SETD2 |
| SF3B1 |
| SFN |
| SFRP5 |
| SFXN2 |
| SHC2 |
| SHQ1 |
| SKOR1 |
| SLC25A33 |
| SLC2A5 |
| SLC30A9 |
| SLC35E1 |
| SLC46A2 |
| SLFN11 |
| SLPI |
| SLX4 |
| SMAD3 |
| SMARCA4 |
| SMC1A |
| SMG9 |
| SMYD3 |
| SPEN |
| SRSF4 |
| SSR4 |
| STAG2 |
| STAT5B |
| STIP1 |
| SUMO1 |
| TADA1 |
| TADA2B |
| TAF5L |
| TAF6L |
| TBX3 |
| TCF25 |

| |
|---|
| TCF7 |
| TERT |
| TET1 |
| TET2 |
| TFAP2B |
| TFAP4 |
| TGFB1 |
| TGFBR2 |
| TJP1 |
| TLE2 |
| TLE3 |
| TMEM50A |
| TNFRSF14 |
| TOP3B |
| TP53 |
| TP73 |
| TRADD |
| TRAF2 |
| TREX2 |
| TRMT11 |
| TRRAP |
| TSC2 |
| TSHR |
| UGT2B28 |
| USP22 |
| VWC2L |
| WDR27 |
| WDR45 |
| WDR49 |
| WDR70 |
| WNT1 |
| WNT3 |
| WT1 |
| WTAP |
| WWTR1 |
| XIAP |
| YIPF7 |
| YWHAZ |
| ZFHX3 |
| ZMYM2 |
| ZNF319 |
| ZNF485 |
| ZNF501 |

| |
|---|
| ZNF527 |

**Table A.4: Genes enriched in Focused SCLC FHSC14-1 screen: Saline.** Table listing all genes found to have either 2 or 3 corresponding sgRNAs enriched in the saline treated tumors relative to the P0.

| 2 sgRNAs Enriched | 3 sgRNAs Enriched |
|---|---|
| ARID1B | ATP6V1G3 |
| ARNT2 | BBS4 |
| BAX | CDK8 |
| CPN1 | DLX3 |
| CYB561D2 | ETV3 |
| DDR2 | HIST1H4L |
| ERBB4 | IRS1 |
| FAT1 | MSH6 |
| GPX3 | SFRP5 |
| GSK3B | TLE2 |
| HEXA | |
| HIST1H3A | |
| LAMA1 | |
| LATS2 | |
| MAP3K1 | |
| MET | |
| MMP26 | |
| NCOR1 | |
| NDUFV3 | |
| NME6 | |
| OTOP3 | |
| PDGFRA | |
| PPP3CC | |
| PREX2 | |
| PRKCI | |
| PTEN | |
| RIPK1 | |
| SLC35E1 | |
| SMG9 | |
| TET2 | |
| TFAP2B | |
| WWTR1 | |
| ZNF485 | |

**Table A.5: Genes enriched in Focused SCLC FHSC14-1 screen: Cis-Eto.** Table listing all genes found to have either 2 or 3 corresponding sgRNAs enriched in the cis-eto treated tumors relative to the P0.

| 2 sgRNAs Enriched | 3 sgRNAs Enriched |
|---|---|
| ALDH3A1 | PPP3CC |
| ARNT2 | PRICKLE1 |
| BBC3 | |
| CPN1 | |
| DOT1L | |
| FLT1 | |
| GPX3 | |
| GSK3B | |
| GSTM5 | |
| HESX1 | |
| HTR6 | |
| KEAP1 | |
| LGALS9 | |
| MET | |
| NSD1 | |
| PLS3 | |
| PRDM14 | |
| SLFN11 | |
| TLE3 | |
| UGT2B28 | |
| USP22 | |
| WWTR1 | |

**Table A.6: Genes enriched in Focused SCLC FHSC14-2 screen: Saline.** Table listing all genes found to have 2,3, or 4 corresponding sgRNAs enriched in the saline treated tumors relative to the P0.

| 2 sgRNAs Enriched | 3 sgRNAs Enriched | 4 sgRNAs Enriched |
|---|---|---|
| ALDH3A1 | ALK | BCOR |
| ALDOA | ALOX12B | CDK8 |
| ANKS1A | AMER1 | DVL2 |
| ARAF | ARNT2 | GLI1 |
| ARID1B | ASXL1 | HIST1H4L |

| | | |
|---|---|---|
| ARID5B | ATM | KCNIP3 |
| ATP6V1G3 | BBS4 | WWTR1 |
| ATRX | CAMSAP3 | |
| BAX | CBL | |
| BCL2L11 | DLX3 | |
| BLM | DNMT3B | |
| BRCA2 | ERBB4 | |
| BRD9 | FANCA | |
| CASP14 | FOXH1 | |
| CASP6 | GRHL1 | |
| CDCP1 | HIST1H3A | |
| CDKN1A | HMOX1 | |
| CDKN2A | INHBA | |
| CDKN2C | JAK2 | |
| CDKN2D | KNSTRN | |
| CLDN11 | MAP2K1 | |
| CPN1 | MAP3K1 | |
| CTNNB1 | MBOAT4 | |
| CUL5 | MGA | |
| CXCL16 | MMP26 | |
| DLC1 | NDUFV3 | |
| DUSP4 | NKX3-1 | |
| ENY2 | NME6 | |
| EPHA7 | NOTCH2 | |
| ESR1 | NOTCH3 | |
| ETV3 | NSD1 | |
| FAH | NTRK3 | |
| FAS | PDGFRB | |
| FAT1 | PIGG | |
| FHL3 | PIK3R1 | |
| FLT1 | PPARD | |
| FLT3 | PPP3CC | |
| FOXF2 | PRDM1 | |
| FOXO1 | SKOR1 | |
| FZD7 | TLE2 | |
| HECW1 | TLE3 | |
| HESX1 | WDR27 | |
| HTR1F | | |
| HUS1B | | |
| IFNA7 | | |
| IGF1R | | |
| INPP4A | | |
| IRS1 | | |

| | | |
|---|---|---|
| ITPRIP | | |
| JAK1 | | |
| KDM6B | | |
| KDR | | |
| KRT27 | | |
| LYN | | |
| MAP3K11 | | |
| MDC1 | | |
| MDM2 | | |
| MID1 | | |
| MSH2 | | |
| MSH6 | | |
| NCOR1 | | |
| NELL1 | | |
| NOTCH4 | | |
| NQO1 | | |
| PALB2 | | |
| PIK3C2G | | |
| PIK3CG | | |
| POGK | | |
| PPP1R12C | | |
| PRDM14 | | |
| PREX2 | | |
| PRKCI | | |
| PTP4A1 | | |
| PTPRT | | |
| RAB8B | | |
| RASA1 | | |
| RBL2 | | |
| RIPK1 | | |
| SFXN2 | | |
| SHC2 | | |
| SLC30A9 | | |
| SLPI | | |
| SRSF4 | | |
| TADA1 | | |
| TBX3 | | |
| TET1 | | |
| TFAP4 | | |
| TJP1 | | |
| TNFRSF14 | | |
| TRAF2 | | |
| TRMT11 | | |

| | | |
|---|---|---|
| TRRAP | | |
| TSC2 | | |
| UGT2B28 | | |
| YIPF7 | | |
| ZMYM2 | | |

**Table A.7: Genes enriched in Focused SCLC FHSC14-2 screen: Cis-Eto.** Table listing all genes found to have 1,2, or 4 corresponding sgRNAs enriched in the cis-eto treated tumors relative to the P0.

| 1 sgRNAs Enriched | 2 sgRNAs Enriched | 4 sgRNAs Enriched |
|---|---|---|
| ATXN7 | TADA2B | TADA1 |
| FAS | USP22 | TAF5L |
| GP6 | | |
| ITPRIP | | |
| KEAP1 | | |
| KLK5 | | |
| MED12 | | |
| RET | | |
| S100G | | |
| SKOR1 | | |
| SLC35E1 | | |
| STIP1 | | |
| TAF6L | | |
| TP73 | | |